

T-3293

THE EFFECT OF STRESS ON THE WELD METAL ACICULAR FERRITE
PHASE TRANSFORMATION

by:

Craig B. Dallam

ARTHUR LAKES LIBRARY
COLORADO SCHOOL of MINES
GOLDEN, COLORADO 80401

ProQuest Number: 10796299

All rights reserved

INFORMATION TO ALL USERS

The quality of this reproduction is dependent upon the quality of the copy submitted.

In the unlikely event that the author did not send a complete manuscript and there are missing pages, these will be noted. Also, if material had to be removed, a note will indicate the deletion.



ProQuest 10796299

Published by ProQuest LLC (2019). Copyright of the Dissertation is held by the Author.

All rights reserved.

This work is protected against unauthorized copying under Title 17, United States Code
Microform Edition © ProQuest LLC.

ProQuest LLC.
789 East Eisenhower Parkway
P.O. Box 1346
Ann Arbor, MI 48106 – 1346

A thesis submitted to the Faculty and the Board of Trustees of the Colorado School of Mines is partial fulfillment of the requirements for the degree of Doctoral of Philosophy (Metallurgical Engineering).

Golden, Colorado

Date 10-10-86

Signed: Craig Dallam
Craig B. Dallam

Approved: David L. Olson
David L. Olson
Thesis Advisor

Golden, Colorado

Date OCTOBER 11, 1986

William D. Copeland
William D. Copeland, Head
Metallurgical Engineering

ABSTRACT

Microstructures comprised of mainly fine grained acicular ferrite are known to be beneficial with regard towards toughness and strength of low carbon steel weld metal. Many attempts have been made to understand the transformation to acicular ferrite. One model suggests that thermal stresses developed adjacent to inclusions promote the nucleation of acicular ferrite. Stresses are prevalent in welding, so the objective of this study was to determine whether stresses of the magnitude attainable in welding alter the nucleation behavior or transformation behavior of weld metal. In particular, the nucleation of acicular ferrite is studied.

A test matrix was developed where a series of all-weld metal samples were put through a temperature cycle typical of what is seen in actual weld using a Gleeble 1500 testing system. Simultaneously, a loading cycle was applied. Both tensile and compressive loading cycles were used, with the maximum loading condition corresponding to the largest tensile stress that can be developed in a fully constrained weld. The test matrix consisted of a series of tests run at fractions of this loading cycle, both in tension and compression.

A second test matrix, nearly identical to the first, was also run. The difference between the two matrices was simply a matter of growing large austenite grains when the Gleeble samples was at its peak temperature, 1370°C. Additional tests were performed where the

sample in various loading conditions were rapidly quenched at various times after the transformation had commenced.

The results collected were temperatures at which the acicular ferrite began to form, and many parameters from quantitative metallography. The volume fractions of various microstructural constituents and prior austenite grain size were measured, but for the analysis of a proposed model, the average acicular ferrite lath size was the most important. This parameter is so important because an assumption is made that the acicular ferrite transformation is controlled by nucleation, so the number of laths per unit volume of material is indicative of the nucleation rate of the acicular ferrite.

The analysis of data centered around an expression for the classical nucleation rate. This expression contains activation energy terms which can be altered in the presence of applied loads. Corrections may then be made to the activation energy terms in the classical nucleation rate expression to account for the effects of the applied loading conditions. Approximations then can be made, and experimentally observed acicular ferrite grain size data can be related to transformation temperatures.

Among the major conclusions of this study are that the effects of changing austenite grain size has a much more profound effect on the nucleation rate (acicular ferrite lath size) than does the applied loading condition. The applied loading conditions have little impact on the microstructure.

TABLE OF CONTENTS

	<u>Page</u>
ABSTRACT	iii
TABLE OF CONTENTS	v
LIST OF FIGURES	vii
LIST OF TABLES	x
ACKNOWLEDGEMENTS	xi
I. Introduction	1
A. Classical Nucleation Theory	2
B. Non-Isothermal Nucleation	7
C. Acicular Ferrite	10
General Background	10
Theories of Nucleation	17
D. Effect of Stress on Austenite Decomposition	25
Macroscopic Applied Stresses	25
Localized Stresses	32
E. Definition of Thesis Problem	41
II. Experimental Procedure	43
III. Results	55
A. Fine Grained Austenite Tests	55
B. Coarse Austenite Grain Tests	64
C. Summary of Results	69
IV. Discussion	70
A. Nucleation in an Unstressed System	71
B. Nucleation with Strain Energy	73
C. Expected Results	77
D. Comparison of Predicted to Actual Results	81
E. Influence of Austenite Grain Size	83
F. Suggested Future Topics	90
G. Summary	91

	<u>Page</u>
V. CONCLUSIONS	93
VI. REFERENCES CITED	94
VII. APPENDIX: Thermal Program Utilized in Gleeble Tests is Presented	101

LIST OF FIGURES

<u>Figure No.</u>	<u>Figure Caption</u>	<u>Page</u>
1	Diagram showing how various contributions to the total free energy vary with the size of nucleus. The surface energy term $4\pi r^2$ is proportional to the surface area of the nuclei, while the driving force for reaction with or without stress decrease with the volume of the nuclei. The activation energy barrier for nucleation ΔG^* and critical nuclei size r^* are shown.	4
2	The relationship between weld metal oxygen content and the basicity index of flux is shown.	12
3	A schematic continuous cooling transformation (CCT) diagram is shown. GF represents grain boundary ferrite SF signifies sideplate ferrite (Widmanstätten ferrite), AF stands for acicular ferrite, B is bainite, and M represents martensite. The final microstructure depends on where the cooling curve intersects the various transformation curves.	14
4	The orientation of experimental samples with respect to the weld is schematically represented.	44
5	This time-temperature-load diagram shows how the first test were performed. After a 3 minute hold the sample was subjected to an experimental cool as the desired loading cycle was applied.	47
6	The manner in which the first test was run is diagrammed. After heating to a peak temperature of 1370°C, the ram on the testing machine is moved to recouple the ram with the sample fixturing then held in place as the sample is allowed to cool.	48
7	Typical experimental data is shown as the sample cools the load increases until ferrite formation causes the load to decrease. The sample diameter, as given by the dilatometer output, shows an opposite trend.	49

<u>Figure No.</u>	<u>Figure Caption</u>	<u>Page</u>
8	The range of loading cycles is displayed, using the actual chart recorder output. These tensile loading cycles, three compressive loading cycles, and one "no load" condition were utilized.	51
9	A typical dilatometer output trace is presented. Point 1 is the minima in dilatometer output and the acicular ferrite begins to form at point 2.	53
10	The acicular ferrite lath size for various loading conditions are given for two austenite grain sizes. An additional point is given for a sample which plastically deformed.	56
11	Typical microstructures for regions of acicular ferrite are shown for fine austenite grained samples in the a) -1.0 (compression) normalized loading condition, b) no load condition and c) +1.0 (tension) loading condition.	57
12	Typical microstructures are shown for a) the fine grained austenite tests and b) the coarse grained austenite tests.	58
13	The prior austenite grain sizes are shown for the "fine" and "coarse" grained austenite samples.	60
14	The variation of percentage of the microstructure compressed of grain boundary ferrite is shown for the different loading conditions.	61
15	The variation of aligned ferrite is shown for the different loading conditions.	62
16	At the various loading conditions, the percentage of acicular ferrite in the microstructure is shown for the two austenite grain size conditions.	63
17	Regions of typical acicular ferrite in the large austenite grain size samples are shown. The compressive loading cycles of -1.0 normalized load is shown in a) in b) the no load condition is shown and in c) is the +1.0 normalized loading condition.	65

<u>Figure No.</u>	<u>Figure Caption</u>	<u>Page</u>
18	The variation of grain boundary ferrite thickness is presented for the different normalized loading conditions and austenite grain sizes.	67
19	The microstructure of the samples was made up of grain boundary ferrite, acicular ferrite and aligned ferrite. Discounting the grain boundary ferrite, the amount of acicular ferrite is shown.	68
20	A schematic diagram is presented of free energy versus reaction coordinate. State 1 is austenite which has G_{γ} , State 2 is ferrite with a free energy of G_{α} . The driving force for reaction is ΔG_v while the atoms passing from austenite to ferrite must overcome the barrier of ΔG° .	72
21	This CCT diagram, after Nilan (49), shows how high compressive stresses push the transformation curves to longer times and lower temperatures.	81
22	The variation of acicular ferrite lath size with austenite grain size is given for the data of Fleck (26).	84

LIST OF TABLES

		<u>Page</u>
1	Nominal compositions of the weld metal from which samples were prepared, and also of the base plate	45

ACKNOWLEDGEMENTS

I would like to thank my advisor, Dr. D.L. Olson, Dr. G.R. Edwards, and Dr. D.K. Matlock for their continued assistance. They have provided common sense and support for things ranging from equipment problems and interpretation of results to swimming around Boulder Reservoir.

The contributions of Brian Damkroger and Dr. E.L. Brown are also acknowledged, as is the input from Dr. J.U. Trefny and Dr. J.T. Brown.

The Army Research Office funded this work.

Lowell Mott of Hobart Brothers Co. has also assisted when called upon.

Additionally, thanks are due to Juan Milian, Dr. S. Liu, Gianluca Beverini, Dr. C.E. Cross, and Mike Maguire.

I. INTRODUCTION

In low carbon steel welds, a microstructure comprised mainly of fine acicular ferrite has been found to be desirable for good strength and toughness properties (1,2). While much has been done to learn about the formation of acicular ferrite (3-10), it is still a subject that is far from being completely understood.

Weld metal, by its very nature, is subjected to stresses. Base plate is usually constrained so after welding the cooling metal develops thermal stresses - the same effects give rise to residual stresses in welds. Additionally, there are many oxide inclusions in weld metal which are important in the development of microstructures. Because of differences in thermal contraction coefficients, thermal stresses arise adjacent to the inclusions. The purpose of this research is to evaluate whether the stresses of the magnitude attainable in steel weld metal can affect the formation of acicular ferrite.

Classical nucleation concepts will be discussed which pertain to the nucleation of acicular ferrite. Background is presented including past observations and theories on the formation of acicular ferrite, and then on existing information of the effect of stress on the decomposition of austenite to ferrite. Both macroscopic and microscopic stresses are mentioned. The effects of applied stresses will be introduced into nucleation theory to modify the classical nucleation expression.

The experimental procedures used here are discussed in a section followed by the results obtained in these tests. Finally there is a discussion of the results. A comparison of the results to those expected from a nucleation model are presented, and finally the effect of austenite grain size on the formation of acicular ferrite is discussed.

A. Classical Nucleation Theory

In metallic systems, diffusion phase transformations occur by nucleation and growth processes, during which stable nuclei of the product phase form and grow by the transport of atoms to the nuclei. Since this is such a common and important topic for the development of the microstructure and properties for materials, the process has often been examined. (11).

In the development of the thermodynamics of nucleation, a strain free system is usually assumed; e.g. forming liquid out of vapor with homogeneous nucleation. In this case, only two factors contribute to the total free energy change of the system, the volume free energy driving the reaction, and the energy contribution from the formation of an interface between the phases. If spherical product particles with radius r are assumed to nucleate, the volume free energy will be proportional to r^3 and the surface energy term will be proportional to r^2 , therefore, the total free energy change may be written:

$$\Delta G_{\text{tot}} = 4/3\pi r^3 \Delta G_v + 4\pi r^2 Y \quad (1)$$

Where ΔG_{tot} is the total free energy change of the system, ΔG_v is the volume free energy change (ΔG_v is less than zero for a spontaneous reaction), and Y is the specific interphase interfacial energy (a positive number). The formation of a stable nucleus occurs in conjunction with a maximum in total free energy with respect to nuclei size. The addition of atoms to the critically sized nucleus decreases the total change in free energy for the system and allows the new phase to grow. By setting the derivative of this expression with respect to r equal to zero, the critical size of a stable nucleus (r^*) can be found to be:

$$r^* = \frac{-2Y}{\Delta G_v} \quad (2)$$

Nuclei smaller than this are not stable, while nuclei above this size lower their free energy by the successive addition of atoms to the nucleus. The value of ΔG^* , the height of the activation barrier for nucleation may be calculated by substituting r^* into the expression for ΔG_{tot} . This yields for the spherical nuclei case:

$$\Delta G^* = \frac{16\pi Y^3}{3\Delta G_v^2} \quad (3)$$

Figure 1 is a schematic representation of the quantities discussed here.

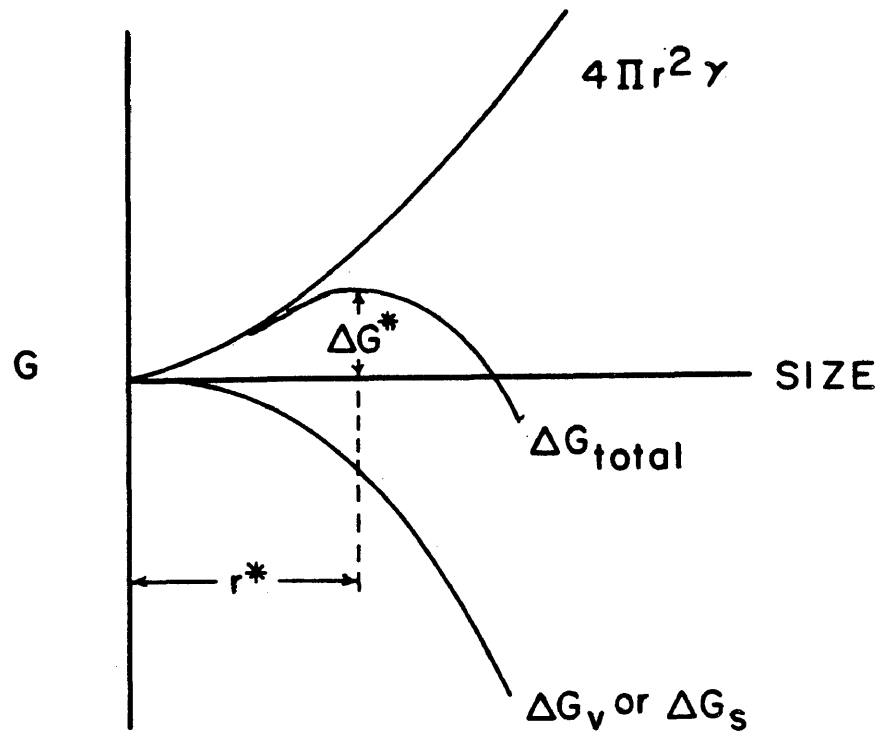


Figure 1. Diagram showing how various contributions to the total free energy vary with the size of nucleus. The surface energy term $4\pi r^2 \gamma$ is proportional to the surface area of the nuclei, while the driving force for reaction with or without stress decrease with the volume of the nuclei. The activation energy barrier for nucleation ΔG^* and critical nuclei size r^* are shown.

In metallic systems, the concept of critical nuclei size remains, but complications arise in the solid state. Parent and product phases rarely have the same specific volume, so in the course of transformation, a transformation strain energy is added to ΔG_{tot} . Transformation strains and induced stresses are generally assumed to be elastic, and the transformation strain energy is proportional to the volume of the nuclei, so the form of the free energy equation then becomes:

$$\Delta G_{\text{tot}} = \frac{4}{3}\pi r^3 (\Delta G_{\text{v}} + \Delta G_{\text{T}}) + 4\pi r^2 \gamma \quad (4)$$

where $\Delta G_{\text{s}}^{\text{t}}$ is the volume strain energy associated with the transformation. The transformation strain energy term is positive. Clearly, if the strain energy is large enough, ΔG_{tot} always exceeds zero, so the reaction will not proceed. The volume free energy may be further modified by the addition of a strain energy term associated with externally applied stresses, $\Delta G_{\text{s}}^{\text{a}}$. The equation for the total free energy change is then written in the following form:

$$\Delta G_{\text{tot}} = \frac{4\pi r^3}{3} (\Delta G_{\text{v}} + \Delta G_{\text{T}} + \Delta G_{\text{s}}^{\text{a}}) + 4\pi r^2 \gamma \quad (5)$$

The externally applied stresses can affect nucleation by changing the specific volume differences between the parent and product phases, or by modifying $\Delta G_{\text{s}}^{\text{t}}$. The applied loads can

also directly affect the strain energy through the elastic or plastic deformation of the parent phase.

At this stage of the analysis, the activation energy barrier to nucleation is:

$$\Delta G^* = \frac{16\pi\gamma^3}{3 (\Delta G_V + \Delta G_T + \Delta G_A)^2} \quad (6)$$

The strain energy terms nominally decreases ΔG^* , however, there can be interactions between the applied and transformation stresses. Applied hydrostatic stresses can assist or counteract the transformation stresses.

In real systems, nucleation rarely occurs homogeneously. Grain boundaries, inclusions and triple points are all sites for heterogeneous nucleation. By forming heterogeneously at these locations, the second phase at these sites can decrease the necessary volume for the critical nucleus and enhance the nucleation rate. Typically, the reduction in activation energy is given as a simple geometric factor that multiplies the homogeneous activation energy barrier. This is given as:

$$\Delta G^*_{het} = \Delta G^*_{homo} (f(g)) \quad (7)$$

Where ΔG^*_{het} is the barrier for heterogeneous nucleation,

ΔG^*_{homo} is the barrier for homogeneous nucleation, and $f(g)$ is a geometric factor.

The expression for nucleation rate is related to several factors, including ΔG^* . The nucleation rate, which is the number of stable nuclei that form per unit volume per unit time, is dependent on many factors. It will be proportional to how many atoms attempt to join a forming nucleus, ν , on how many atoms are in a position to join a forming nucleus, 0_c . Also it will be related to the probability of an atom being transported into the forming nucleus which is dependent on ΔG° , the activation energy barrier to diffusion across an austenite/ferrite interface. Additionally, the nucleation rate will be dependent on how many potential nucleation sites are available, N_o , and the probability that one of these is available for the neighboring atoms to join in. This is given by equation 8.

$$I = \frac{dN}{dt} = 0_c \nu \exp \frac{-\Delta G^\circ}{RT} N_o \exp \frac{\Delta G^* f(\xi)}{RT} \quad (8)$$

B. Non-Isothermal Nucleation

The classical nucleation rate expression given in equation 8 was developed for an isothermal conditions. Welding is a continuous cooling processes, so the classical nucleation rate expression will not be quantitatively accurate. By differentiating the equation, then integrating with respect to temperature, a general expression valid for non-isothermal nucleation may be found.

Continuous nucleation in a non-isothermal system can be viewed as an incremental nucleation process. For continuous cooling, a fractional amount of nucleation can be thought of as happening in every temperature increment as the temperature decreases. When the fractional amount of nucleation has reached a value large enough to be determined experimentally, nucleation is complete. This procedure has been used to create continuous cooling transformation diagrams from isothermal transformation data (12).

When the sum of the fraction of time to nucleation occurring at each temperature on the cooling cycle equals one, nucleation will have occurred. This can be expressed in equation form as:

$$1 = \int_{N/No = 0}^{N/No = 1} d\left(\frac{N}{No}\right) \quad (9)$$

where N is the number of nuclei that have formed and No is the total number of possible nucleation sites. Furthermore, when this condition is met, the expression for classical nucleation will contain the critical time and temperature for nucleation. This expression is complicated because of the temperature-time relationship and the form of the classical nucleation expression and is given as the following expression:

$$1 = \int_t^{t_n} N_o^0 c^v \left[\exp \frac{-\Delta G^0}{RT(t)} + \frac{A\gamma^3 T_{eq}^2}{\Delta H^2 (T(t) - T_{eq})^2 T(t)} \right] dt \quad (10)$$

Where A is a geometric term, γ is the interfacial energy, T_{eq} is the equilibrium temperature, ΔH is the enthalpy change, and ΔG^0 is the barrier to atom motion across into the nucleus.

The origin of this particular form using ΔT instead of ΔG^* is given later in the Discussion section and the temperature is given as $T(t)$ to point out that it is a function of time. The term t_n is the time to nucleate. This equation could be solved numerically provide sufficient information of the physical parameters were available.

Qualitatively, non-isothermal nucleation can still be understood by looking separately at the effects of time and temperature. Nucleation is not a process that can be totally described by a single time for a certain temperature. Rather there is a distribution of times over which nucleation occurs. As indicated by the exponential nature of the activation energy, the number of nuclei forming per unit time (the rate of formation of stable nuclei) varies with time. Initially there will be a very low rate of nucleation and at extremely large times (the actual time depends on the temperature) there will be a maximum in the nucleation rate.

C. Acicular Ferrite Formation

General Background

The factors affecting the toughness and strength of microalloyed HSLA steel weld metal are important since these steels need to be welded prior to service. The nature of the toughness-microstructure relationship has then been a subject of interest (13-24). Among the original observations pertaining to the toughness of these weld metals was the "vectorial approach" of Garland and Kirkwood (14) where the base properties were either improved or hindered by various factors such as precipitation hardening, grain refinement, and solid solution strengthening. Using many flux-wire combinations for submerged arc welding to obtain a wide range of weld compositions, they observed several metallurgical variables affecting the toughness and strength of the weld metal. The main toughening mechanism was found to be the formation of acicular ferrite at the expense of blocky ferrite along prior austenite grain boundaries. Because of the refined grain size, the acicular ferrite caused an increase in both strength and toughness. This is the fundamental basis for microalloying technology, that mechanical property improvements due to grain refinement outweigh the effects of factors such as precipitation hardening. The effect of several alloying elements was examined, but the effect of oxygen on microstructure was ignored.

Tuliani, Boniszewski, and Eaton (15), examined the effect of flux basicity on the properties of weld metal. The basicity index, BI, given in equation 11 was developed to measure sulfur removing capability of a slag, and is the ratio of basic components to acidic components. Although developed for sulfur, many of the components act similarly with regard to oxygen. Because of this, the basicity index is often related to weld metal oxygen content, especially for calcium silicate type fluxes. Furthermore, weld metal strength and toughness depend on weld metal oxygen content, so there can be an indirect effect between the basicity index and properties. Figure 2 shows how the weld metal oxygen varies with basicity index. Improvement in mechanical properties was attributed to the cleanliness of the weld pool.

$$BI = \frac{CaO + CaF_2 + MgO + K_2O + Na_2O + Li_2O + 1/2 (MnO+FeO)}{SiO_2 + 1/2 (Al_2O_3 + TiO_2 + ZrO_2)} \quad (11)$$

Garland and Kirkwood (16) demonstrated the interdependence of flux basicity, weld metal oxygen content, microstructure, and the resulting toughness of the weld metal. They also observed that high heat inputs prevent the formation of acicular ferrite microstructures. Taylor and Farrar (17) reported that inclusions were responsible for the mechanical properties of weld metal, but did not see them as being important in the development of fine

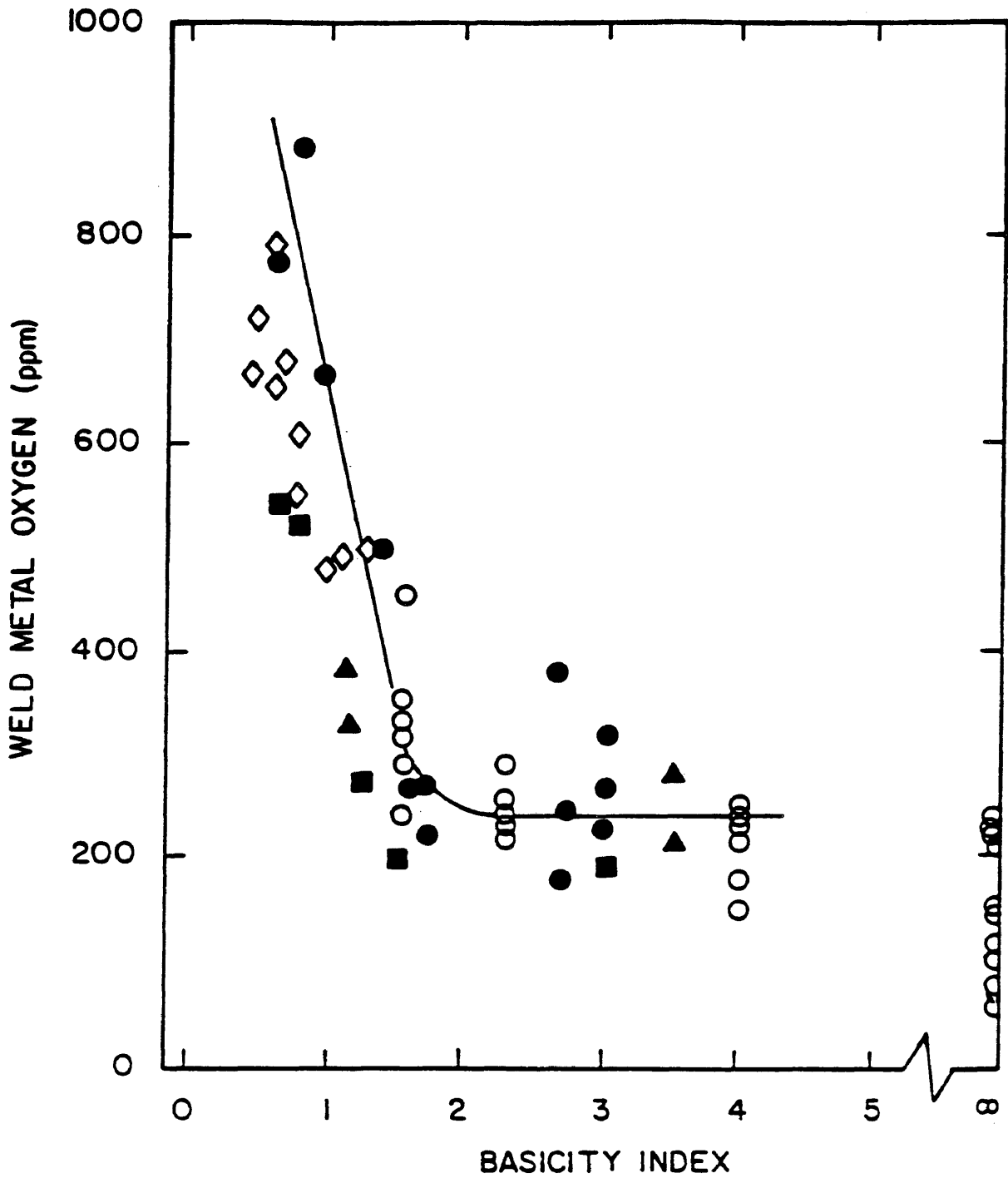
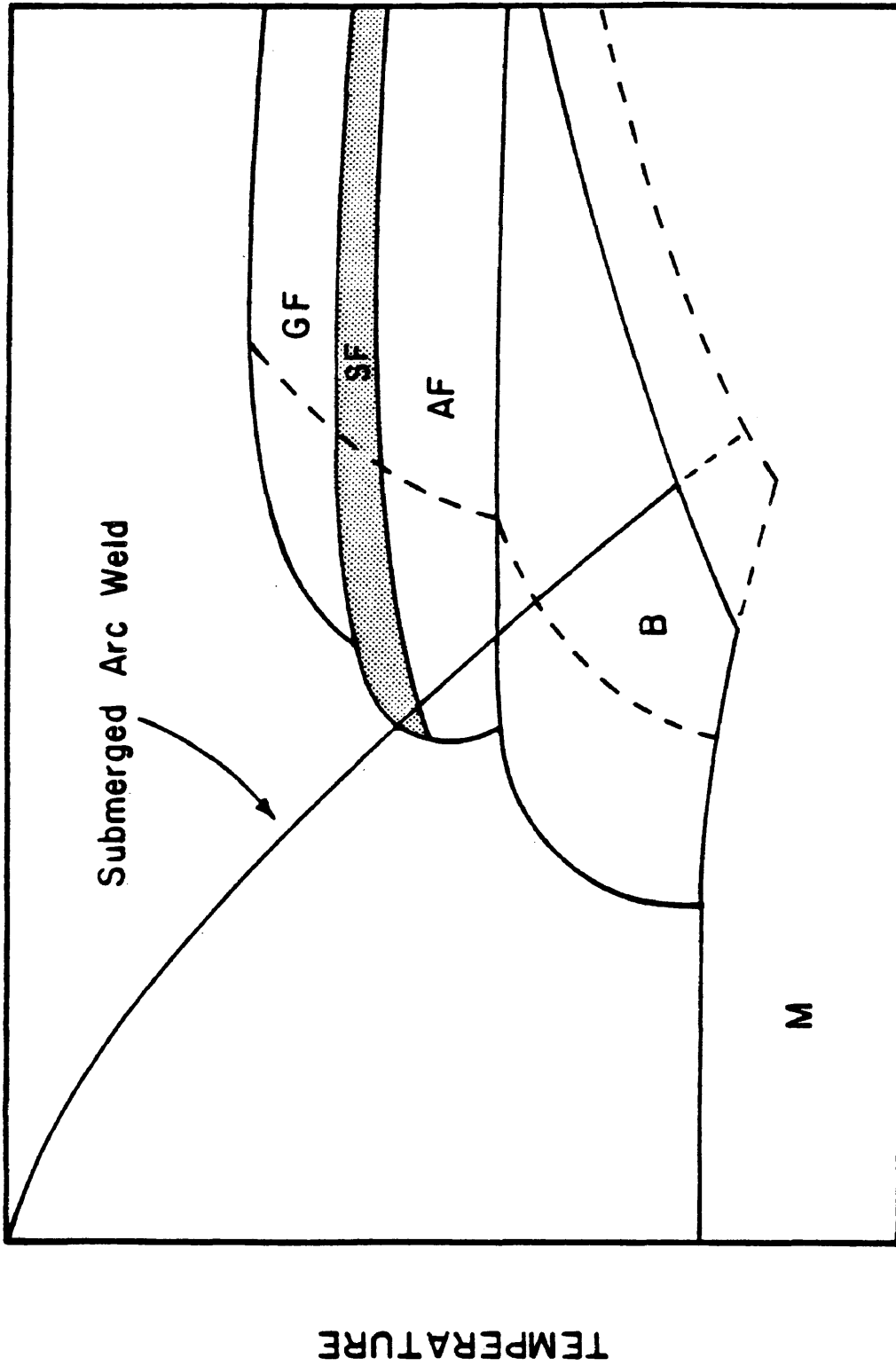


Figure 2. The relationship between weld metal oxygen content and the basicity index of flux is shown.

grained microstructures. Heat input to the weld was viewed as critical in determining the toughness of the weld metal, but they found that the optimum acicular ferrite microstructure at a given heat input depended on the flux used.

Thomas (18), Evans (19), Glover, et al. (20) and Levine and Hill (21) have suggested that acicular ferrite formation could be represented with continuous cooling transformation (CCT) diagram concepts where the hardenability of the weld metal and the cooling rate of the metal can be related to the formation of acicular ferrite. Figure 3 shows a schematic CCT diagram which can be used to show the effects of various cooling rates and compositions on the transformation behavior. The effect of oxygen on the continuous cooling transformation diagram is to move the curves opposite to the direction in which hardenability agents move the curves, making the ferrite products form at shorter times.

Dallam, Liu, and Olson (22) demonstrated how weld metal oxygen variations could produce a variety of microstructures. Using fluxes of the $\text{CaF}_2\text{-CaO-SiO}_2$ system, a wide variety of weld metal oxygen contents could be obtained with essentially constant bulk weld metal compositions. With very low weld metal oxygen contents, bainitic microstructures formed. As the oxygen content in the weld metal increased, predominately acicular ferrite microstructures would result, and as the amount of oxygen continued to increase, so did the percentage of grain boundary ferrite. The optimum oxygen



LOG TIME

Figure 3. A schematic continuous cooling transformation (CCT) diagram is shown. Grain boundary ferrite (GF), Widmanstatten sideplate ferrite (SF), acicular ferrite (AF), bainite (B), or martensite (M) may be present in the final microstructure depending on where the cooling and transformation curves meet.

content, providing the highest proportion of acicular ferrite was around 280 ppm.

Koukabi, North, and Bell (23) examined the effects of small percentages of zirconium, vanadium, titanium, and boron on the microstructures of submerged arc welds. The role of weld metal oxygen had been viewed as somehow promoting the formation of grain boundary ferrite, so reducing the weld metal oxygen content would promote acicular ferrite. Zirconium deoxidizes the weld metal without promoting acicular ferrite. Titanium and vanadium additions promoted acicular ferrite, while zirconium did not, so it becomes apparent that the nature of inclusions promote the transformation to acicular ferrite.

Bhadesia, Svensson and Gretoft (24) developed a scheme by which the microstructures of Fe-Mn-Si-C weld metal could be explained. This was done by looking at each of the individual reactions that occur in these materials, one at a time, using conventional phase transformation theory. It was possible, knowing the austenite grain size, composition, and cooling rate to calculate the isothermal transformation diagrams and the quantities 1) initiation time and 2) time to completion for each of the particular phase transformations. Allotriomorphic (grain boundary) ferrite always forms first, and the amount in the final microstructure depends on how fast the allotriomorphs thicken, and also the amount of austenite grain boundary available on which it may nucleate. The

volume fractions of both Widmanstätten ferrite (an aligned ferrite growing out of the allotriomorphic ferrite) and acicular ferrite depend on how much can form before impinging on the grain boundary ferrite. The relative rates of formation of the intergranular and grain boundary products is therefore also important. Acicular ferrite was seen to need inclusions in order to nucleate, and a minimum weld metal oxygen content of 250 ppm was suggested. The growth rates of the allotriomorphic ferrite and Widmanstätten ferrite were found to be hindered through the addition of alloying elements. They suggest that the initial formation of allotriomorphic ferrite may control the further development of the microstructure during subsequent cooling.

Liu (25) looked at the development of grain boundary ferrite films using Avrami transformation kinetics theory. Assuming that grain boundary ferrite nucleates easily and grows in a direction perpendicular to the interface, and estimating a transformation time and parabolic growth rate constant, he could estimate the volume fraction of grain boundary ferrite for several grain sizes. A good correlation was found between experimental and estimated volume fractions of grain boundary ferrite.

Fleck et al. (26) also looked at the development of microstructures in Fe-Mn-Mo-Nb steel weld metal using a variety of consumables. Their main conclusion dealt with the importance of inclusions in controlling the austenite grain size, and the

subsequent effect on the final microstructure. Using Avrami kinetics for plane front transformation, they predicted how the amount of acicular ferrite decreased with increasing austenite grain size. Although not explicitly mentioned in their paper, a trend was seen of increasingly finer acicular ferrite laths resulting from increasing austenite grain sizes. With their consumables, an acicular ferrite lath size of over two microns resulted from 76 micron austenite grains, and this decreased significantly to 1.5 microns when the austenite grain size was slightly over 100 microns. A compositional parameter P_{cm} , developed by Ito and Bessyo, was correlated with the volume fraction of acicular ferrite. This parameter is:

$$P_{cm} = C + \frac{Mn + Cu + Cr}{20} + \frac{Si}{30} + \frac{Ni}{60} + \frac{Mo}{15} + \frac{V}{10} + 5B \quad (12)$$

Higher hardenability (P_{cm}) yielded larger amounts of acicular ferrite. An increase from 0.18 to 0.21 in P_{cm} netted an increase in the volume fraction of acicular ferrite from 26 to 80 percent.

Inclusion Nucleation - Background

Abson, et al. (3) offered the first hypothesis that acicular ferrite forms heterogeneously on second phase particles in the austenite. By lowering the oxygen content from several hundred parts per million in weld metal to 100 ppm the transformation to

acicular ferrite was virtually eliminated. Acicular ferrite was viewed as a proeutectoid ferrite with individual grains forming on the available heterogeneous nucleation sites. Oxides can promote grain boundary ferrite if present near grain boundaries, or acicular ferrite if present inside austenite grains. Abson found that equivalent 600 ppm weld metal oxygen contents generated using two different fluxes, one calcium silicate and the other alumina based, resulted in drastically different microstructures. This suggests the nature of inclusions make them effective as nucleation sites for acicular ferrite. Abson concluded that the inclusion type and size distribution were far more important than the total oxygen content or inclusion volume fraction in determining the microstructure of the weld metal.

Cochrane and Kirkwood (4) demonstrated, using dilatometry, that high oxygen weld metal transformed from austenite to ferrite at higher temperatures than low oxygen weld metal. They noted that the size distribution of particles would be very important in terms of affecting transformation behavior.

Choi and Hill (5) used steels containing manganese and molybdenum to study submerged arc weld metal transformations. The grain boundary ferrite was found to form between 1000°C and 750°C; Widmanstätten ferrite formed between 750°C and 650°C. Acicular ferrite started forming at about 600°C. All transformation was complete at a temperature of 500°C.

Ricks, Howell and Barritte (6) studied the nature of the acicular ferrite transformation. In their tests, welds were quenched during the cooling cycle after the ferrite transformation had started. This allowed the existing ferrite microstructure to be retained in regions of martensite. Using E7018 welding rods, austenite grain boundaries always were saturated with allotriomorphic ferrite before acicular ferrite formed. On the basis of transmission electron microscopy (TEM) observations, acicular ferrite was seen to be much the same as Widmanstätten ferrite. Retained austenite and twinned martensite were observed adjacent to acicular ferrite laths. This is indicative of a high carbon concentration in these regions. Carbon must have been rejected by the growing acicular ferrite rather than precipitating internally as in the case for bainite. Stepped interfaces were often observed between the ferrite and retained austenite, suggesting a stepwise growth for the thickening of the acicular ferrite laths.

Effects of Austenite Grain Size on Ferrite Transformation

One mechanism by which oxides may control the amounts of acicular ferrite, grain boundary ferrite, and other microstructural features is through the control of the austenite grain size. After solidification of the weld, austenite grains can coarsen. If an appropriate inclusion dispersion is present, the extent of coarsening may be limited. Weld metal with low oxide content can

have austenite grains coarsen substantially in comparison to high oxygen weld metal. With small austenite grain sizes, there is a large amount of austenite grain boundary area per volume of metal. Since grain boundaries act as the nucleation sites for allotriomorphic ferrite, fine austenite microstructure would be expected to promote allotriomorphic ferrite at the expense of acicular ferrite.

Keville and Cochrane (7) discussed the role of inclusions in the development of weld metal microstructures. They viewed inclusions as effective substrates for delta ferrite upon solidification. The temperature at which the inclusions form can have an effect on the microstructure since this will, at least indirectly, determine the size distribution of the inclusion after solidification. Barrite and Edmonds (8) presented evidence of nucleation of acicular ferrite on inclusions and also observed the critical interdependence of inclusion content and austenite grain size. Acicular ferrite formed only after the austenite grain boundaries were saturated with ferrite.

Liu (25) showed that the prior austenite grain size was directly related to the amount of oxygen in the weld metal. Austenite grain size was seen to decrease from 100 microns at 100 ppm weld metal oxygen to 70 microns at 500 ppm oxygen, and the fraction of grain boundary ferrite increased from 7 to 20 percent with this grain refinement. Liu also observed that the size

distribution of inclusions is important in two ways: small inclusions are more effective at pinning the austenite grain boundaries, while large inclusions are more effective heterogeneous nucleation sites for acicular ferrite. Liu and Olson (28) determined the optimum inclusion size distribution to achieve weld metal with high fractions of very fine acicular ferrite.

Harrison and Farrar (9) showed that high weld metal oxygen contents tended to produce fine austenite grains size. This favors the formation of higher temperature transformation products at the abundant austenite grain boundaries. Farrante and Farrar (10) found that austenite grain sizes over 45 microns were sufficiently large for acicular ferrite to form.

One theory of how inclusions limit the growth of grains is that of Zener (29). He showed the limiting grain size, D_1 , as:

$$D_1 = \frac{2d}{3f} \quad (13)$$

where d is the average particle size and f is the volume fraction of inclusions. D_1 would be the largest an austenite grain could grow. For example, the driving force for the grain growth is the minimization of grain boundary surface energy, and capillarity forces ultimately limit the grain growth. One implication of this is that for a given weld metal oxygen content, small inclusions are more effective at limiting the austenite grain size than are large

inclusions than large inclusions. Small inclusions provide a much higher surface area per volume of inclusions. Growing grains must then do more work to overcome the obstacles.

Further refinements to this theory have been made. For example, Gladman (30) developed an expression for the critical inclusion size which is too large to limit grain growth. The form of this expression is:

$$d_{cr} = \frac{3Df}{\pi} \frac{1}{\left(\frac{3}{2} - \frac{2}{Z}\right)} \quad (14)$$

where d_{cr} is the largest inclusion that will prevent grain growth, and f is the volume fraction of inclusions. Z is the ratio between a growing grain size diameter and the matrix grain size. D is the matrix grain size.

In summary, inclusions affect the evolution of weld metal microstructures by controlling the microstructural scale and by providing attractive heterogeneous nucleation sites for acicular ferrite.

Effect of Lattice Disregistry on Nucleation of Acicular Ferrite

Ito and Nakanishi (31) studied microstructures in titanium and boron microalloyed steel weld metal. They found that acicular ferrite would often nucleate on titanium nitride particles. Mori, Homma, Okita, and Wakabayashi (32) determined that in titanium and

boron microalloyed steel weld metal the boron prevents allotriomorphic ferrite from forming, and found that titanium oxide instead of titanium nitride acted as the nucleation sites for the acicular ferrite formation. They attributed the potency of titanium oxides to the lattice disregistry between the oxide and the ferrite. Crystalline particles with good atomic matching across the oxide-ferrite interface promote heterogeneous nucleation. Lattice disregistry is a factor which modifies the potency for heterogeneous nucleation.

Effect of Localized Thermal Stresses

Recognizing that some characteristic of the inclusions had an effect on the acicular ferrite transformation, Devillers, et al. (33) added small amounts of various elements to the weld metal to systematically change the characteristics of the second phase particles. Along with admitting the potential effects of lattice disregistry and heterogeneous nucleation, (and possibly local compositional differences immediately adjacent to the inclusions), they proposed a model in which the difference in thermal contraction coefficients between the inclusion and austenite cause high local stresses that promote acicular ferrite. Following solidification, an inclusion will fit perfectly into the metal matrix surrounding it. As the metal cools, the inclusion and matrix contract different amounts, thereby setting up stresses.

In a different context, the magnitude of stresses brought on by thermal contraction of inclusions and its energy was studied by Brooksbank and Andrews (34). These stresses are described in equation form as:

$$\sigma = \phi (\alpha_i - \alpha_m) \Delta T \quad (15)$$

where ϕ is a function of the elastic moduli of the inclusion and the matrix, α_i and α_m are the coefficients of thermal expansion of the inclusion and the austenite respectively, and ΔT is the degree of undercooling.

This is the "ball in the hole" problem which has been examined in detail in other situations (35,36). This problem arises in dislocation theory when looking at either a substitutional element atom in a matrix, or a precipitate forming in a matrix. Hirth and Loethe (35) examined this problem and came up with expressions for isothermal pressure and stresses associated with the ball in the hole. The displacement of the ball can be determined knowing proper material properties and the energy associated with the "ball in the hole" can be calculated knowing this information.

D. Effect of Stress on Austenite Decomposition

Macroscopic Applied Stress

The effect of applied stress on the decomposition of austenite has been generally to increase the rate of transformation to ferrite. Most work that has been done in this area has been on the decomposition of austenite to ferrite-pearlite in plate steels. Studies (37-47) have shown that both uniaxial tension and compression accelerate the transformation, while other studies (48-51) to be described later show that hydrostatic pressure retards the transformation from austenite.

According to Nocke in Denis, et al. (37) isothermal transformation curves are displaced to shorter times when subjected to stress. Nocke showed that tensile and compressive stresses of the same magnitude have essentially the same effect on altering the transformation kinetics. The acceleration of the transformation under tension was explained in terms of the modification to the free energy by the strain energy. Microplasticity has been reported to promote heterogeneous nucleation (37).

Walker and Honeycombe (38), examining chromium-molybdenum-nickel steels and 0.2 weight percent carbon - 5.0 weight percent chromium steels, found that the effect of prior work on the austenite was to increase the rate of nucleation and to promote intragranular ferrite. Deformation produced a finer microstructure, and intragranular ferrite was seen to form on deformation bands in the samples.

Smith and Siebert (39) worked with low carbon molybdenum steel plate with small amounts of boron. In undeformed specimens, additional alloying lowered the limiting cooling rates to avoid the formation of polygonal ferrite. The same effect was seen with deformed samples, but the limiting cooling rate to avoid polygonal ferrite was increased with the amount of prior work. Once again, the effect of prior work was to accelerate the transformation to ferrite. The limiting cooling rate increased exponentially with true strain in the austenite. However, with increasing strain the austenite eventually recrystallized so the transformation slowed to that of the undeformed specimens. The transformation of low carbon austenite after small plastic strains was studied by Priestner and Biring (40). Hot deformation of a 0.1 weight percent carbon steels and a 0.1 weight percent carbon, 1.5 weight percent manganese, 0.04 percent niobium steel hastened the transformation to ferrite and softened the transformation product. The high hardenability of the high manganese steel resulted in austenite recrystallization prior to transformation and therefore slowed the transformation rate.

Ducoin, et al. (41) looked at the influence of stress on plain carbon steels of various carbon contents and a medium alloy steel and found an acceleration of transformation under tensile stress. Mutiu, et al. (42) worked with AISI 4340 steel and found that the effect of stress was to accelerate the transformation, and also produced a finer bainite lath size.

Bhattacharyya and Kehl (43) used AISI 1085, 4340 and 1045 steels to study the isothermal decomposition behavior of austenite to bainite under stresses. Various temperatures ranging from 280°C to 370°C were used as tensile stresses as high as 60,000 psi (413 MPa) were applied. The tensile stresses reduced both the transformation start and completion times by factors ranging from 2 to 100,000 depending on steel and the temperature. For a given time the amount of austenite transformed increases greatly at a stress range corresponding to the yield stress of the unstable austenite. The amount of austenite transformed at any time can be correlated with the amount of plastic strain and applied strain energy. Under high stress conditions the coarseness of bainite was reduced, and it was suggested that this was due to an increased nucleation rate.

The same authors later examined (44) the effect of stress upon the transformation to pearlite using AISI 1085 and 10B45 steel. Stresses of 13000 psi (89.5 MPa) were used and isothermal transformation proceeded at 1273°F (690°C) and 1253°F (678°C) respectively. Applied stress markedly accelerated both the beginning and end of transformation times. By examining the transformation kinetics, the nucleation rate was found to have increased by a factor of over fifty. This is based upon the time required to initiate the transformation, after initiation the time to completion, however, was not strongly affected. In the AISI 10B45 steel the nucleation rate of ferrite doubled, while the growth

rate increased by a factor of 2.5. But this increased growth rate was found only in the later stages of transformation.

Porter and Rosenthal (45) looked at the eutectoid steels to determine how applied loads affected the transformations to pearlite, bainite and martensite. Their experimental set up consisted of a dead weight load on a wire specimen. Electrical resistance and extension of the wire sample could be continuously monitored. They found that stress in excess of a critical value accelerates the pearlite and bainite transformation and raises the martensite start temperature. Plastic extension of the samples accompanies the transformation from austenite when the threshold stress has been applied. They viewed dislocation pileups as being locations for nucleation of bainite and pearlite.

Priestner (46) examined the strain induced transformation to ferrite in HSLA steels. During rolling, the strain induced transformation to ferrite occurred along elongated austenite grain boundaries and deformation bands, producing a fine ferrite grain size. In some cases extremely large ferrite grains which were heavily substructured formed. Allotriomorphic ferrite grains that nucleated prior to rolling may have rotated to create these large grains.

The transformation to pearlite from a work hardened eutectoid austenite was presented by Umemoto, Ohtsuka and Tamura (47). They deformed austenite below the recrystallization temperature, then

isothermally transformed the steel. The amount of plastic deformation markedly accelerated the austenite to pearlite transformation, the acceleration being attributed to an increased nucleation rate with an unchanged growth rate. The increase of nucleation rate was attributed to three factors: 1) the increase of austenite grain surface by the elongation of grains, 2) the increase of the nucleation rate itself, and 3) the addition of nucleation sites such as annealing twin boundaries and deformation bands. The inherent nucleation rate increase was determined through their tests to accelerate the transformation the most. An expression was derived for the increase in grain boundary area with rolling reduction, and with this an Avrami type kinetic equation was developed to predict the time for transformation.

Evidence exists that applied stress affects the nucleation rate much more than the growth rate. Denis, et al. (48) reported that high hydrostatic pressures stabilize the austenite and retard the formation of ferrite and cementite.

Nilan (49) looked at the effect of high pressure on austenite decomposition in 0.44 weight percent carbon and 0.82 weight percent carbon steels and molybdenum alloyed steels. The effects of pressures of up to 30 kbar (3000 MPa) were investigated. The most significant of his results was that the hydrostatic pressure increased the hardenability of the steels. In plain carbon steels, the nose of the CCT curve was moved from 0.6 seconds to 600 seconds

by the increase of pressure from ambient to 24 kbar (2400 MPa). Microstructures obtained under these pressures were bainitic and pearlitic, and were morphologically similar to the microstructures obtained under ambient conditions. It was found that the high pressure had different effects on the pearlitic and bainitic reactions, when comparing the molybdenum alloyed steel to the plain carbon steel. The bainite reaction proceeded almost identically at atmospheric pressure and under high pressure in both steels, but the alloyed steel had an increase in pearlite transformation start time of a factor of fifty. The kinetics of transformation were in all cases slowed by increased pressure.

An analysis of these experiments was done using the Johnson-Mehl equation. Since the transformation start times were increased, the nucleation rate was seen to be decreased, and the process of forming a nucleus was assumed the same as growing the nucleus. The Johnson-Mehl equation for diffusion controlled, three dimensional growth is:

$$f = 1 - \exp\left(-\frac{\pi I g^3 t^4}{3}\right) \quad (16)$$

where f is the fractional transformation, I is the nucleation rate, g is the growth rate, and t is the time. By taking the volume transformed as a constant at the start of transformation under pressure and at one atmosphere, the effect of pressure could be

examined by looking at the exponential terms with and without pressure. The energy barriers to nucleation were found assuming that the total free energy change due to pressure was simply a pressure times a change of volume term. The ratio of the activation energy barriers with and without pressure are given by the equation:

$$\frac{\Delta G^*_o}{\Delta G^*_s} = \left(1 - \frac{Pv^*}{\Delta G^*_o}\right)^2 \quad (17)$$

The activation energy barrier to nucleation was seen to be:

$$\Delta G^*_s = \Delta G^*_o + Pv^* \quad (18)$$

where ΔG^*_s includes the effect of pressure, ΔG^*_o does not include the effects of pressure, P is the pressure, and v^* is the activation volume. This information was used to carry out the derivation, where eventually the ratio of times to start the transformation with and without pressure was given by:

$$\frac{t_p}{t_o} = \left(\frac{I_o(g_o)}{I_p g_p^3}\right)^{1/4} = \left(1 - \frac{Pv^*}{\Delta G^*_o}\right)^{-1/2} \exp\left(\frac{P(v^*+1/4i^*dv)}{kT}\right) \quad (19)$$

where t_p and t_o are the times for the transformation to start with and without pressure, I_o and I_p are nucleation rates without and with pressure, P is the pressure, dv is the volumetric change upon transformation, i^* is the size of the nucleus, and v^* is the activation volume. The ratio of the transformation start times

is shown to be exponentially dependent on the pressure. A 1000 atmosphere (101 MPa) pressure is seen to delay the transformation by only twenty five percent, while a 30000 atmosphere (3040 MPa) pressure delays the start of transformation by a factor of 1000 times.

Other studies of high pressure austenite decomposition include studies by Fujita and Suzuki (50), and Radcliffe, Schatz, and Kulin (51), who each observed that the applied pressures delayed the transformation. Some morphological differences were seen in bainite formed under high pressures compared to the low pressure samples.

Effect of Localized Stresses on Phase Transformations

Stresses can be developed on very local levels from at least two sources in metals, 1) the difference in specific volume of parent and product phase, and 2) from differences in thermal contraction. Stress concentrations at singularities can also occur when a macroscopic stress is applied.

The role of the strain energy has been examined by many investigators (52-63). The first generalized solution was by Eshelby (52), who found the elastic energy associated with a particle inside a matrix. A precipitate rarely has the same elastic properties as the matrix it forms from, so an elastic field is associated with the particle. Thermal expansion differences, phase transformations or twinning can all cause stresses.

Expressions have been developed describing the energy associated with transformation. If anisotropic properties are accounted for, the equations become extremely cumbersome, and only the most generalized solutions can be handled numerically.

The initial approach of Eshelby to this problem assumed isotropic materials (both matrix and precipitate) and that the precipitate is ellipsoidal. His method was to consider a series of imaginary cutting, straining and welding operations. Starting with an infinite matrix, he cut out the ellipsoidal region to be transformed, allowing the transformation to occur unconstrained. Surface tractions were then applied to the particle to bring it back to its original shape. This transformed material now just fits into the original hole, the stress equals zero in the matrix and equals a known value in the particle. The system is then allowed to relax.

The total strain energy associated with the matrix and inclusion is given by the expression:

$$E_{el} = -0.5 \int P_{ij}^T e_{ij}^T dv \quad (20)$$

where P_{ij}^T is the stress in the inclusion, e_{ij}^T is the strain in the inclusion, the ij subscripts signify that these are second order tensors, and the integration is over the entire volume of the inclusion. In the case of a uniform expansion, the form of the equation becomes:

$$E_{el} = \frac{2\mu(e^T)^2 v (1+v)}{9(1-v)} \quad (21)$$

where μ is the shear modulus of the inclusion and v is Poisson's ratio. If there is an inclusion of different elastic constants than the matrix and it undergoes a transformation strain of e^T , expressions exist for the strain in the matrix and the inclusion.

The total stored energy will be partitioned between the matrix and inclusion as follows:

$$\frac{E_{mat}}{E_{inc}} = \frac{\mu_{inc} (1-\Omega)}{\mu_{mat} \Omega} \quad (22)$$

where μ is a measure of how well the matrix accommodates strain, and is related to an elastic constant. The term Ω is the ratio of the bulk modulus of the precipitate to that of the matrix.

Many modifications have been made to the work of Eshelby to make the analysis of having two rigid spherical inclusions in close proximity, which changes the stored energy and the stress concentration factor in an infinite solid (53-54).

Chen and Young (55) considered the elasticity problem of a linear elastic, homogeneous, and isotropic matrix and inclusion, but the inclusion could be any arbitrary shape. The next modification came from Lee, Barnett, and Aaronson (56), who dealt with coherent ellipsoidal precipitates in an anisotropic solid. Johnson, Earmme, and Lee (57) derived an equation for inhomogeneous, isotropic precipitates.

By 1977, the only numerical results that had ever been obtained were those of the isotropic case by Robinson (58), Barnett, Lee, Aaronson, and Russell (59), and Shibata and Ono (60). Lee, Barrett, and Aaronson incorporated the elastic strain energy into the minimization process for calculating the nucleation activation barrier with an orientation dependent interfacial energy and elastic strain energy. The shape of the precipitate is then considered. In the isotropic, homogeneous case the strain energy is given by:

$$\Delta G_s = 2\mu \frac{(1+\nu)}{(1-\nu)} \epsilon^2 \quad (23)$$

The ratio of the strain energy of a spherical precipitate to the volumetric free energy needs to be large, on the order of 0.8, for a nucleus to deviate from spherical. They gave the critical energy for nucleation as:

$$\Delta G^* = \frac{\pi\gamma^3 (2+g(\beta))^3}{12\beta(\Delta G_{vol} + \Delta G_s)^2} \quad (24)$$

where β is the aspect ratio of the ellipsoidal precipitate, and $g(\beta)$ is the geometric term to adjust for the orientation dependence and shape dependence of the surface energy of the precipitate. ΔG_s is the strain energy of the inclusion. This can be seen to be the same as given previously by classical nucleation theory, with the modification of the strain energy and the geometric term.

Lee, Earmme, Aaronson, and Russell (61) assumed ideal plastic behavior for an isotropic matrix containing a misfitting spherical precipitate and calculated the total work done during the elasto-plastic deformation and compared this to the total energy in the purely elastic case. This analysis allows for a plastic zone to surround the precipitate. In the large precipitates of over 1000 A, plastic relaxation can account for up to a forty percent reduction in energy for a three percent misfit in the sphere. For particles over a micron in diameter, the most likely nucleation sites, plastic deformation can account for a fifteen percent reduction in strain energy for a three percent misfit.

Following a derivation by Christian (11), Lee, et al. (61) found the total stored energy under elastic conditions to be:

$$E_{el} = \frac{6\mu\alpha\gamma\epsilon^2}{\alpha(\gamma-1)+1}; \quad (25)$$

where

$$\alpha = \frac{1+\nu}{3(1-\nu)} \quad (26)$$

where μ is the shear modulus of the matrix, ν is Poisson's ratio, and Ω is the ratio of the bulk modulus of the precipitate compared to that of the matrix.

If reasonable numbers are inserted for alumina particles in austenite, an assumption is made that no transformation on plastic deformation gas occurred, the stored energy can be up to roughly twenty percent as large as the volumetric free energy. If plastic

deformation is taken into account as well as high temperature recovery, this number should decrease significantly.

In the case where plastic deformation is allowed, the total energy will come from four sources, the elastic energy in the inclusion, the elastic energy of the plastic zone, the plastic energy of the plastic zone, and the elastic energy outside the plastic zone. The governing equation is:

$$E_{\text{tot}} = \frac{p^2}{2\Omega K} (1-\gamma) + \frac{\sigma_y^2}{\alpha u} (1/6 + (r_p/a)^3 \ln(r_p/a)) \quad (27)$$

where p is the equilibrium pressure on the particle, σ_y is the yield stress of the matrix, K is the bulk modulus of the matrix, and r_p/a is the ratio of the plastic zone radius to that of the inclusions.

Lee and Johnson (62) derived an equation for the elastic strain energy associated with precipitates of arbitrary shape in an infinite matrix. The precipitate could be subjected to both stress free transformation strains and uniformly applied strain. This is a further refinement on the analysis of Eshelby (52). With this analysis, the transformation strain energy can be incorporated directly into the calculation for the free energy for formation of a critical nucleus. The interaction between transformation and applied stresses was analyzed using equivalency relationships.

The transformation strain energy W , was represented for a unit volume of precipitate as:

$$W = \frac{1}{2} (\epsilon_{Kl}^{t*} - \epsilon_{Kl}^c) C_{ijkl}^* \epsilon_{ij}^{t*} \quad (28)$$

where ϵ_{Kl}^{t*} is the transformation strain, ϵ_{Kl}^c is strain on a confined system, C_{ijkl}^* represents the elastic constants of the infinite matrix, and ϵ_{ij}^{t*} is the stress free transformation strain. When this is accounted for in the calculation for the activation energy barrier to nucleation, the form of the barrier is:

$$\Delta G^* = \frac{\pi \gamma^3}{12\beta^2} \frac{[2+g(\beta)]^3}{(\Delta G_v + W)^2} \quad (29)$$

In this equation, β is the aspect ratio of the nucleating precipitate, γ is the orientation independent interfacial free energy, ΔG_v is the volumetric free energy change upon transformation, and W is the transformation strain energy. The remaining term is $g(\beta)$, a geometric function related to the surface area of the ellipsoidal embryo, given by:

$$\begin{aligned} & \frac{2\beta^2}{1-\beta^2} \tanh^{-1} (1-\beta^2) \quad \text{if } \beta < 1 \\ & 2 \quad \text{if } \beta = 1 \\ & \frac{2\beta^2}{1-\beta^{-2}} \sin^{-1} (1-\beta^{-2}) \quad \text{if } \beta > 1 \end{aligned} \quad (30)$$

Among the effects of the stress is that precipitation can occur with certain crystallographic or orientation relationships. Lee and Johnson mentioned the results of Lowthian (63) where titanium hydride plates form with broad faces of the plates perpendicular to the tensile axis with stresses approaching 207 MN/m^2 , and also of Hosfor and Agrawal (64) where 48 MN/m^2 compressive stresses along the [100] direction cause θ to precipitate in Al-4% Cu alloys on (010) and (100) planes. Tensile stresses cause precipitation to occur on (001) planes while with no stress all (100) planes are suitable for θ' precipitation.

The actual size, shape and arrangement of precipitates does not depend only on the strain energy, but also on interfacial energy, growth kinetics, applied stresses, and the precipitate input.

Equivalence between the transformation strains and applied strain was also discussed by Lee and Johnson (62). They found the elastic strain energy per unit volume of ellipsoidal precipitate. This accounts for the strain induced by the transformation as well as inhomogeneity stress (due to differences in elastic constants between matrix and precipitate). This was given by W,

$$W = \frac{1}{2} (\epsilon_{K1}^{T*} - \epsilon_{K1}^c - \epsilon_{K1}^A) C_{ijkl}^* \epsilon_{ij}^{t*} - \frac{1}{2} \epsilon_{K1}^A C_{ijKl} \epsilon_{ij}^T \quad (31)$$

where the terms are the same as earlier, and ϵ_{K1}^A is the strain due to the applied stress.

Morris, Khachaturyan and Wen (65) also concerned themselves with how elastic energy pertained to phase transformations. By treating the parent and product phases as linear elastic bodies, many of the consequences of elastic strain can be predicted. Beginning with the "strong harmonic model" of solid solution, both microscopic and macroscopic formulations of linear elastic theory may be developed. The "strong harmonic model" looks at the energy change associated with putting a solute atom in a solid solution. This changes the average composition, C_p , and the position of solute atoms. The change in free energy is then adequately represented by a harmonic series:

$$\begin{aligned}
 \Delta G[U(r), C_p(r)] &= G_0 + \sum_{pr} \phi_{(p)} C_p(r) \\
 &+ \frac{1}{2} \sum_{pr} \sum_r \phi_{pq}(r-r') C_p(r) C_q(r') \\
 &+ \frac{1}{2} \sum_{pr} \sum_{r'} d_l^p(r-r') C_p(r) U_i(r') \\
 &+ \frac{1}{2} \epsilon_{r,r'} \phi_{ij}(r-r') u_i(r) u_j(r')
 \end{aligned} \tag{32}$$

so first order effects are used, then corrected by 2nd order terms and so on.

This is finally given as:

$$\Delta G_{\text{ext}} = V \sigma_{ij} (\epsilon_{ij}^{\text{el}} + \epsilon_{ij}) = V \sigma_{ij} \epsilon_{ij} \tag{33}$$

where ϵ_{ij} is the total strain and V is the volume of the crystal.

For the case of macroscopic inclusions (as opposed to substitutional atom) the elastic strain field and elastic energy can also be found. The external stress (for the macroscopic inclusion) adds the contribution to the free energy $\Delta G(\sigma)$ of

$$\Delta G(\sigma) = V\sigma_{ij} - \epsilon_{ij}^{el} + V_p \sigma_{ij} \epsilon_{ij} \quad (34)$$

where ϵ_{ij} is the invariant plane strain.

Summary of Modifications to Classical Nucleation by Stress

The formation of acicular ferrite in weld metal has been found to depend on how austenite decomposes heterogeneously on inclusions. Various models have been proposed as to how the acicular ferrite proceeds. Macroscopic applied stresses alter the austenite decomposition in plate steels, accelerating the reaction except in the case of hydrostatic compressive stresses. Several treatments of the effect of localized stresses on nucleation processes are available, although they are not practical for numerical analysis except when using simplifying assumptions concerning isotropic properties.

E. Definition of Thesis Problem

The intent of this project is first to find whether stresses attainable in conventional weld metal are sufficient to alter the

acicular ferrite phase transformation behavior. A model has been proposed as to how applied loads should affect the average acicular ferrite lath size. A secondary, but necessarily important aspect of this research is to attempt to explain how prior austenite grain size can influence the acicular ferrite transformation.

II. EXPERIMENTAL PROCEDURE

The experimental program was designed to utilize all-weld metal samples and recreate the welding thermal experience.

Simultaneously, a desired loading cycle could be applied. Rods of weld metal were machined for use on a testing machine that can run concurrent thermal and mechanical cycles.

A niobium microalloyed steel (Lukens Frostline) was submerged arc welded with Oerlikon OP121TT flux and an ER70S-3 electrode. A heat input of 115 kJ/in (4.53 kJ/mm) at 29.5 volts and 550 amperes was used, yielding welds of sufficient penetration in the 0.75 inch (19 mm) steel plate. Cylindrical rods of 0.4 inch (10 mm) in diameter were then machined longitudinally out of the weld metal, as shown in Figure 4. These rods were made in both 6 inch (152 mm) and 4.5 (114 mm) inch lengths, and were threaded on each end. A few of the rods were drilled to give tubes of 4 mm inside diameter. The composition of the weld metal is in Table I.

The threaded rods were of proper size to fit in the 10 mm hot jaws on the Gleeble 1500 testing machine. The Gleeble is a closed loop thermal-mechanical testing system that resistance heats the sample, and the mechanical cycle can either be a stroke, load, or stress. The computer-controlled thermal and mechanical cycles are run by programming desired values for temperature and mechanical mode. For any given time interval, the program sets the value of temperature and either stress, load, or stroke where the sample will

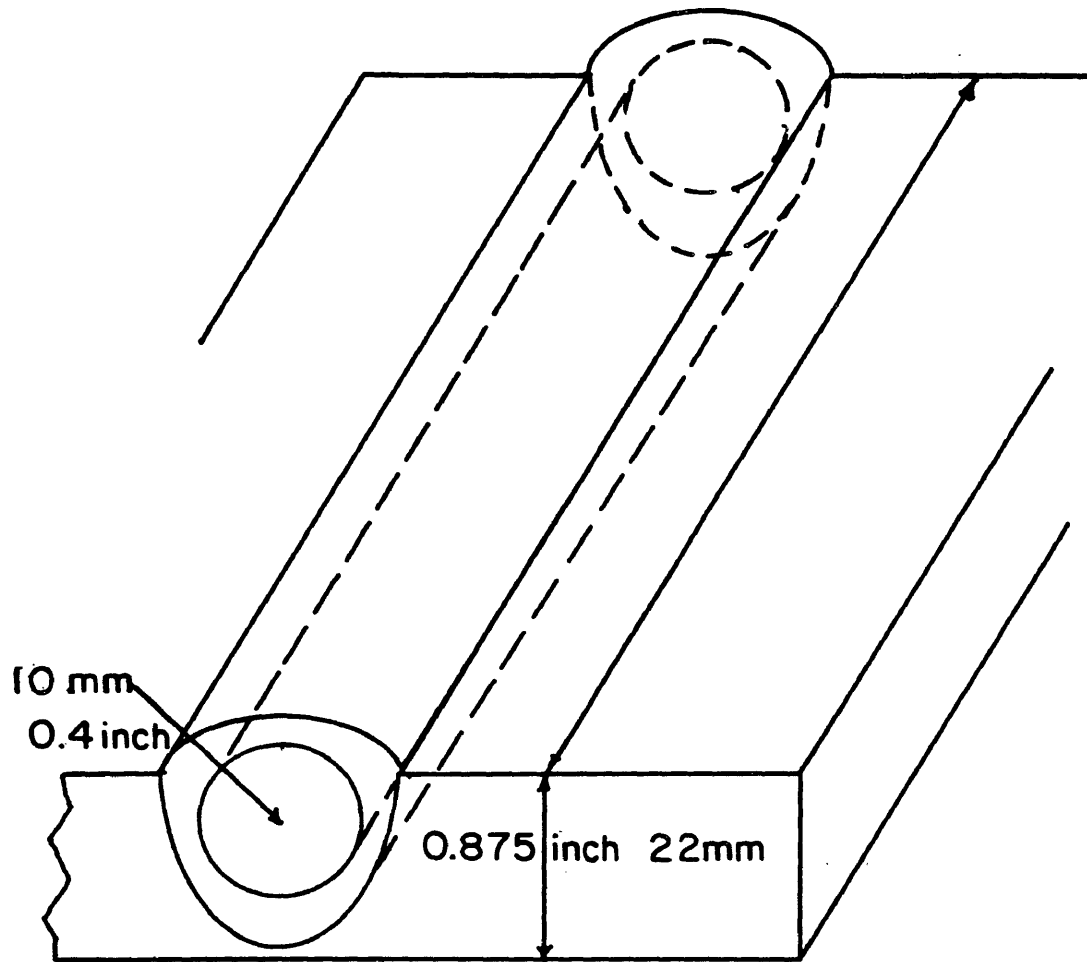


Figure 4. The orientation of experimental samples with respect to the weld is schematically represented.

**TABLE I - Nominal Compositions of the Base Plate Used and
of the Weld Deposits**

	C	Mn	Si	P	S	Cr	Ni	Nb	O	N
Weld Metal	.12	1.19	.412	.0143	.0224	.0752	.0452	.0141	.0211	.0094
Base Plate	.14	1.38	.41	.005	.030	.11	.14	.042	.0083	.0090

be at the end of the time interval, and uses a feedback signal to adjust the values accordingly. Most of the tests used a single cooling cycle, which is presented in Appendix A. The typical thermal cycle consisted of a 10°C per second heat up to a peak temperature of 1370°C , followed by a three minute hold at peak temperature, then an exponential cool with a time to cool from 800 to 500°C of 150 seconds. This is shown in Figure 5.

The first test was run in the following manner: the sample was heated to the peak temperature (1370°C). Under manual control of the mechanical (stroke) cycle. Figure 6 shows the process schematically. As the temperature rises, the sample thermally expands, so at high temperatures the crosshead is no longer coupled with the ram. Under manual control, the ram can be moved to reconnect with crosshead and fix the position. The sample is now locked into position in its peak temperature. Next, as the temperature decreases, longitudinal tensile stresses develop. Figure 7 shows how the load varies in the sample as the temperature. Dilatometer output is also shown. This load profile corresponds the flow curve before the transformation commences and after it is complete.

The normalized load does not strictly correspond to the maximum tensile stress because the peak temperature was 1370°C rather than the melting temperature of the alloy, so less thermal contraction was possible. The stresses corresponding to these normalized loads

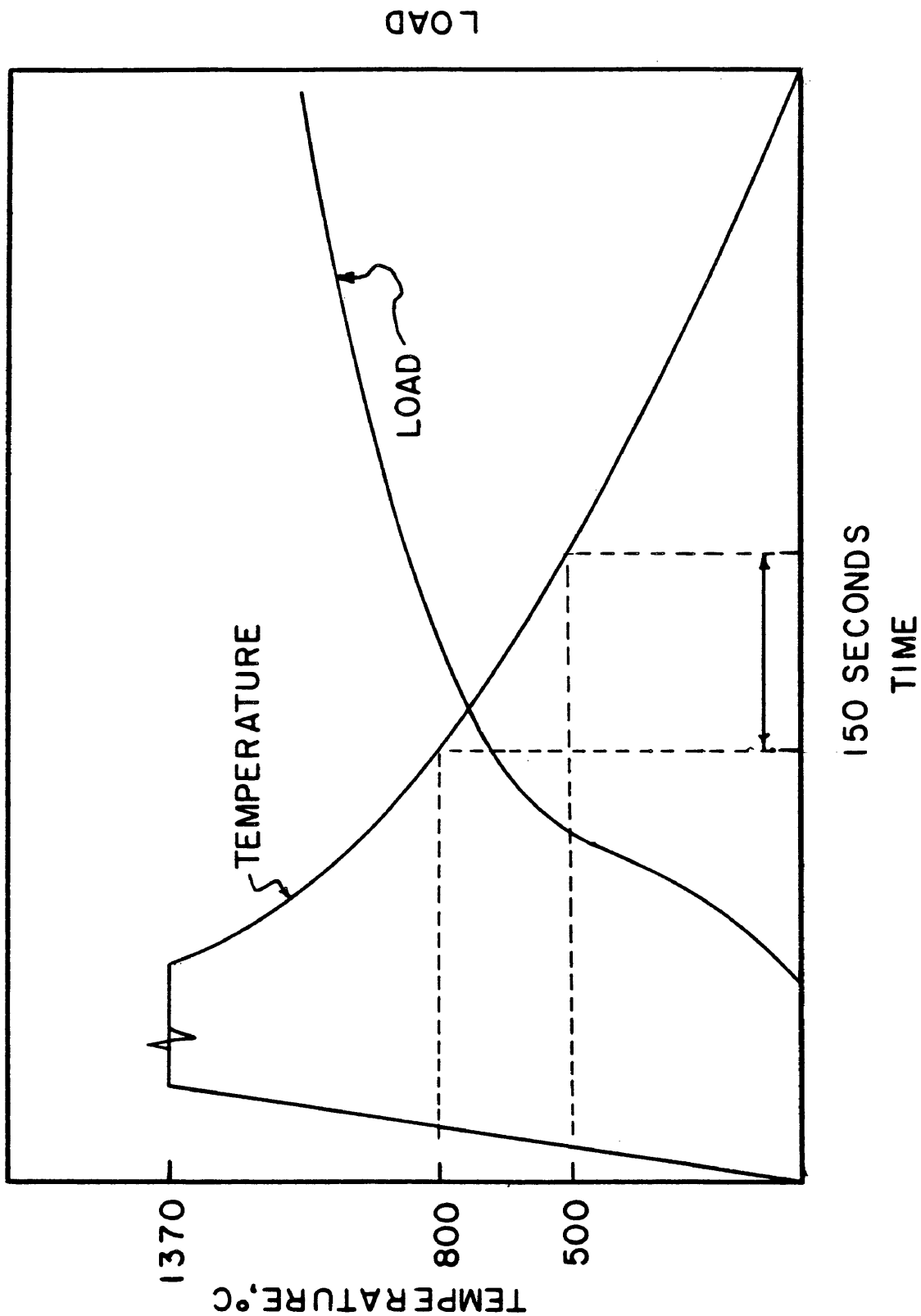


Figure 5. This time-temperature-load diagram shows how the tests were performed. After a 3 minute hold the sample was subjected to an exponential cool as the desired loading cycle was applied.

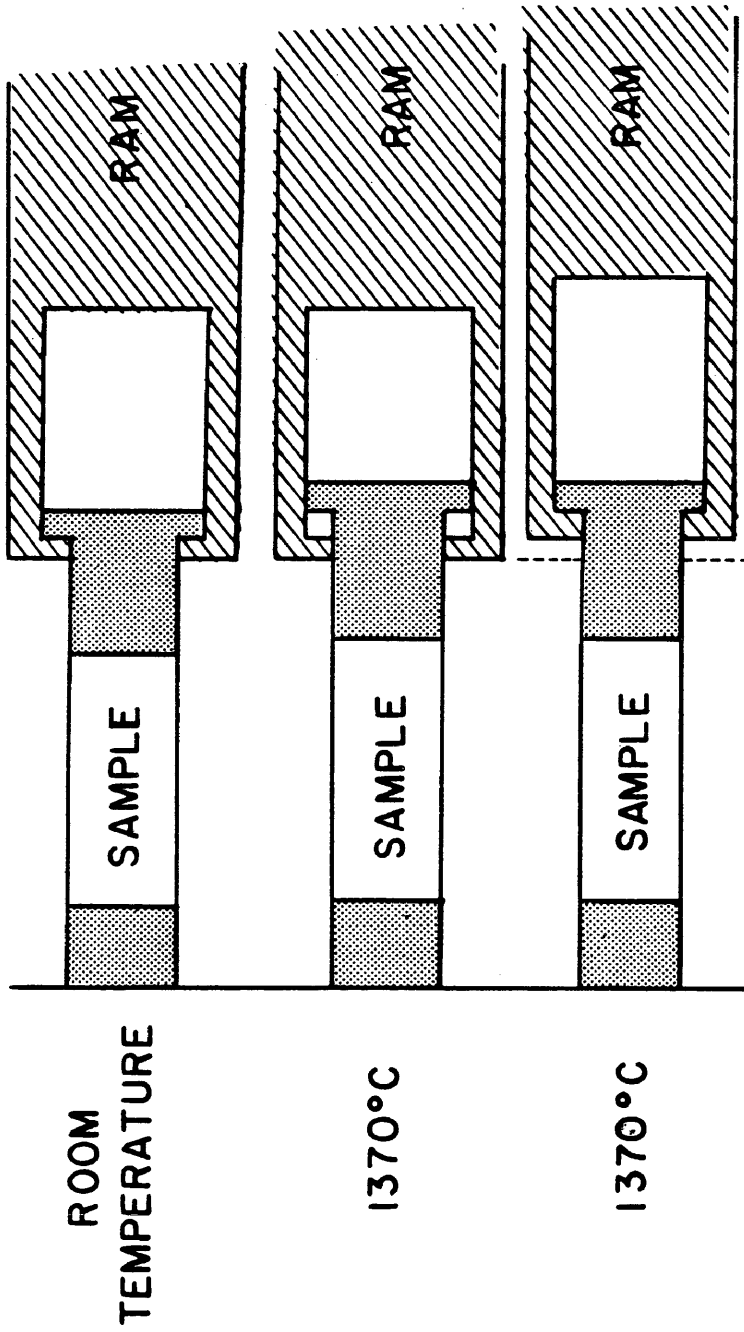


Figure 6. The manner in which the first test was run is diagrammed. After heating to a peak temperature of 1370°C, the ram on the testing machine is moved to recouple the ram with the sample fixturing then held in place as the sample is allowed to cool.

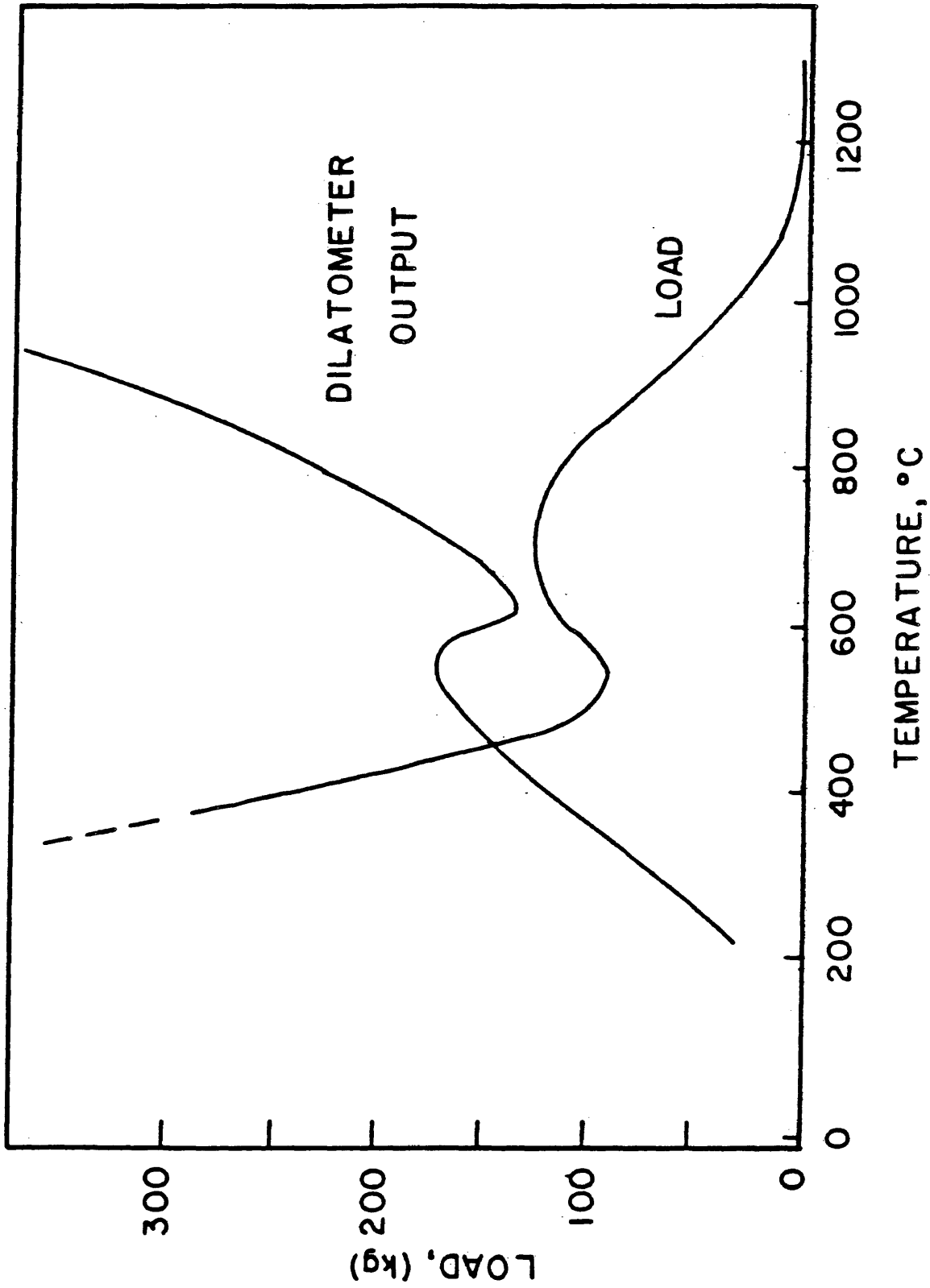


Figure 7. Typical experimental data is shown. As the sample cools, the load increases until the ferrite transformation begins. The sample diameter shows the opposite trend.

are approximately 4250 psi (29 MPa) for the normalized load labelled 1.0 and 4250 psi (29 MPa) compression for the load labelled -1.0 when the sample was in the temperature range 640°C to 575°C.

With this data of the applied load at any point in the time-temperature cycle a set of tests can be generated by multiplying the load at any time-temperature point by 1.0, 0.75, 0.50, 0.0, -0.50, -0.75, and -1.0. These tests are run under load control on the Gleeble testing system. The negative sign corresponds to compressive loading cycles, and the family of loading curves comprise the test matrix. This is shown in Figure 8.

A second test matrix was run very similar to the first, with the exception that an austenite grain growth step was added. A longitudinal strain of three percent was imposed after 40 seconds at the peak temperature followed by three minute hold at 1370°C, after which the thermal and mechanical cycles were run in a manner similar to the previous matrix. The three percent longitudinal strain corresponds to a ten percent circumferential strain at midspan of the Gleeble sample because of thermal gradients in the bar. There is a uniform temperature region in the heated sample, but near the jaws of the Gleeble thermal mechanical testing machine the temperature is not as high.

Each Gleeble specimen was run with a radial dilatometer attached to assist in determining critical temperatures. The chart recorder on the Gleeble thermal mechanical testing machine allows

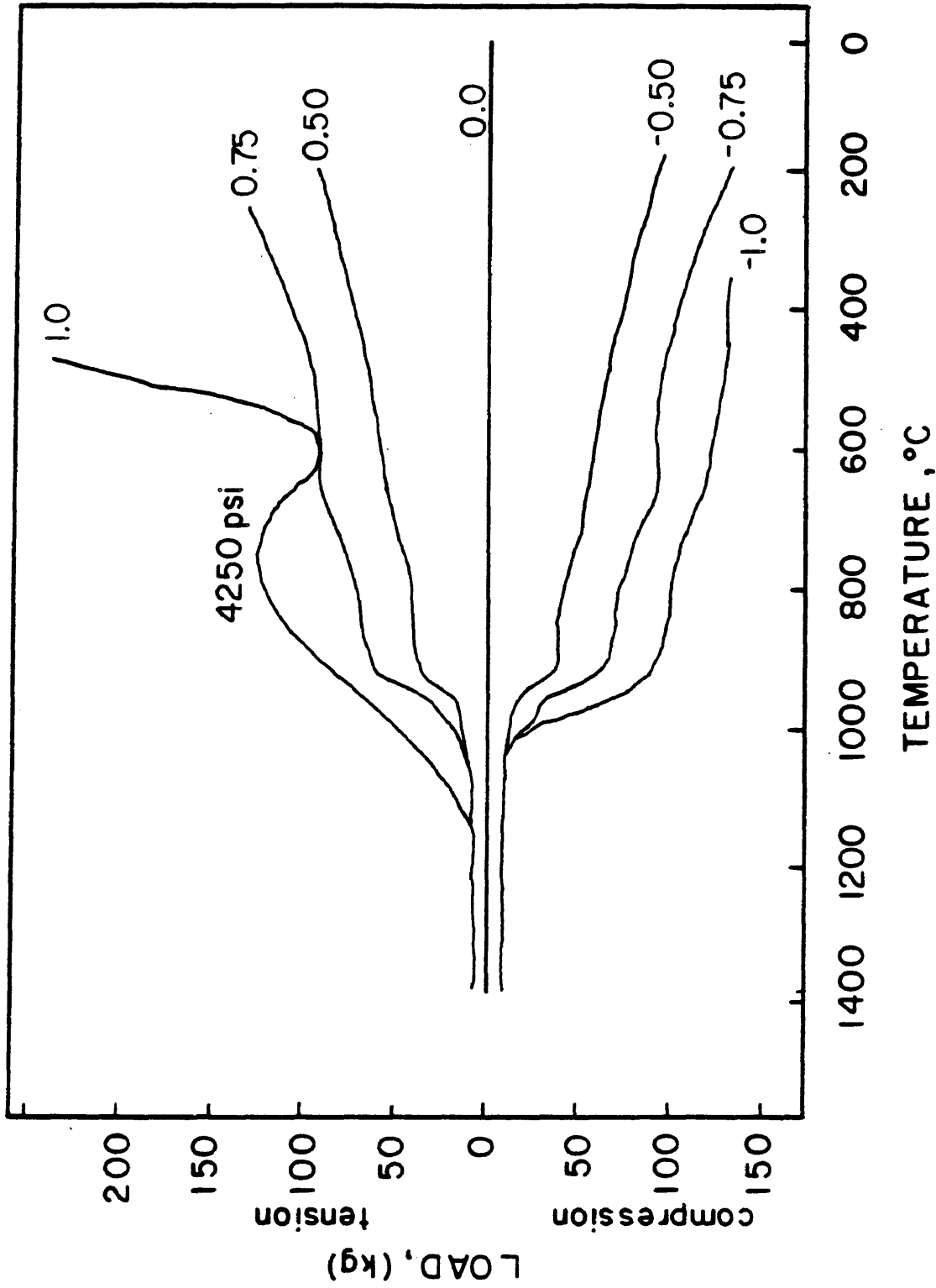


Figure 8. The range of loading cycles is displayed, using the actual chart recorder output. These tensile loading cycles, three compressive loading cycles, and one "no load" condition were utilized.

simultaneous monitoring of load, temperature, programmed temperature, and dilatometer output.

The dilatometer output can be used to determine the transformation temperatures. This is traditionally done by locating where the slope of the dilatometer against either time or temperature changes. The quench tests described earlier were necessary in conjunction with the dilatometer to determine approximate acicular ferrite transformation temperatures. At the minima in dilatometer output, point 1 in Figure 9 the microstructure contains allotriomorphic ferrite coating prior austenite grain boundaries with perhaps a very small amount of Widmanstatten ferrite. It is not until the dilatometer output begins the rapid increase at point 2 in figure 9 that the intragranular laths of acicular ferrite were observed.

Equilibrium temperatures were found through the slow heating of a bar. By heating at 4°C per minute, the A1 temperature was found to be 650°C and the A3 temperature, where the structure becomes entirely austenitic, was found to be 950°C.

The tube samples were tested with identical thermal mechanical cycles as the first test matrix in the maximum tensile, maximum compressive and no load conditions. Cross-sectional differences were considered. However, during the austenite to ferrite transformation, the samples were rapidly cooled with an internal water quench. Through this process, the progress of the transformation could be monitored metallographically.

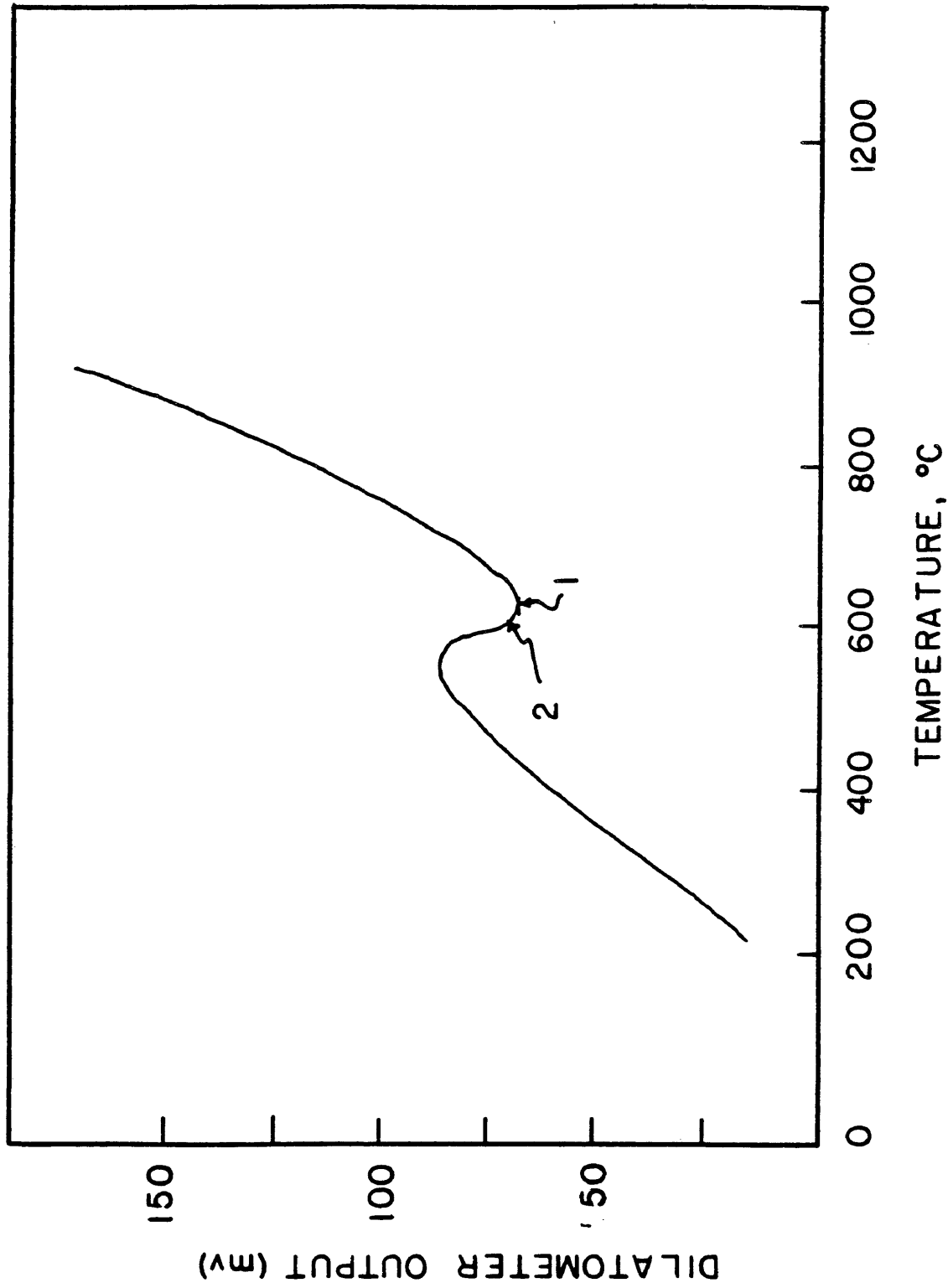


Figure 9. A typical dilatometer output trace is displayed. Point 1 is the minima in dilatometer output, and the acicular ferrite begins at point 2.

Standard metallographic techniques were utilized in the determination of prior austenite grain size, acicular ferrite lath size, and volume fractions of the various ferrite morphologies. Samples were polished to 0.05 μ m followed by a 2% Nital etch. A grid was used to find volume fractions of the various microstructural constituents and line intercepts were used for the ferrite grain size measurement on appropriately magnified samples.

III. RESULTS

The results are most easily presented in two distinct parts, the first pertaining to the "fine grain" austenite tests, and secondly to the "large grain" austenite.

A. Fine Grain Austenite Tests

Two families of data are shown in Figure 10, the top curve being of concern here. The figure is a plot of the acicular ferrite lath size as a function of applied load. The load is given in normalized units ranging from -1.0 to over 1.0. This load scale arises from the manner in which the tests were performed. Refer to the experimental procedure for a more complete description of how the tests were performed, but this scale is most easily thought of as the load normalized to the maximum uniaxial tensile stress that can be developed in a fully constrained weld at any temperature.

The average acicular ferrite lath size was determined from point counts done in regions where only acicular ferrite was present.

The top curve in Figure 10 shows a trend of increasing acicular ferrite lath size as the load increases from a normalized load of -1.0 to a normalized load of +0.0. The increase was from an average lath size of 4.8 μm to roughly 5.4 μm . Typical microstructures are shown in Figure 11 and 12a. As the normalized loading increases to +1.0, the acicular ferrite lath size decreases to about 5.0 μm . One additional point is presented where even higher loads

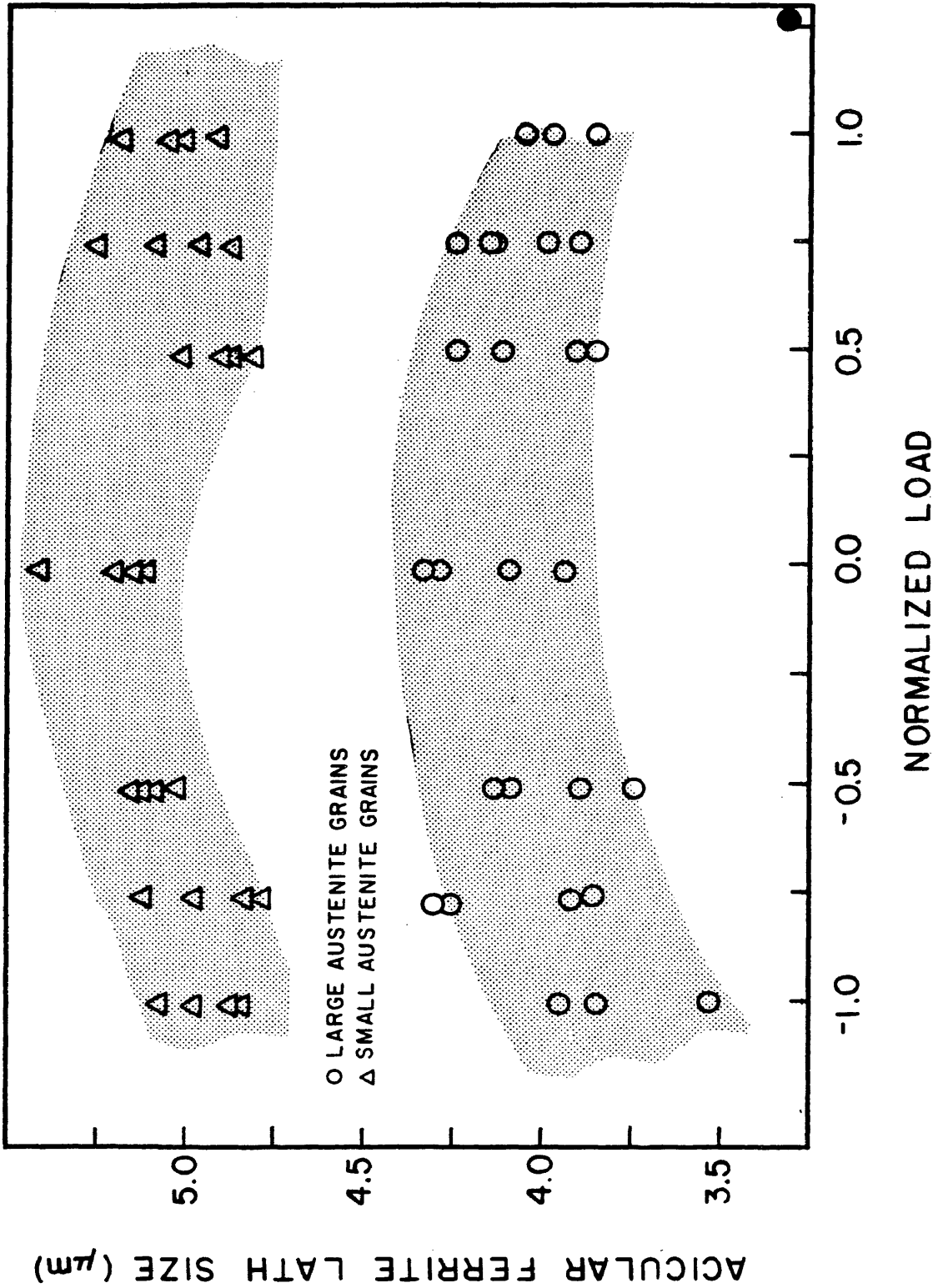


Figure 10. The acicular ferrite lath size for various loading conditions are given for two austenite grain sizes. An additional point is given for a sample which plastically deformed.

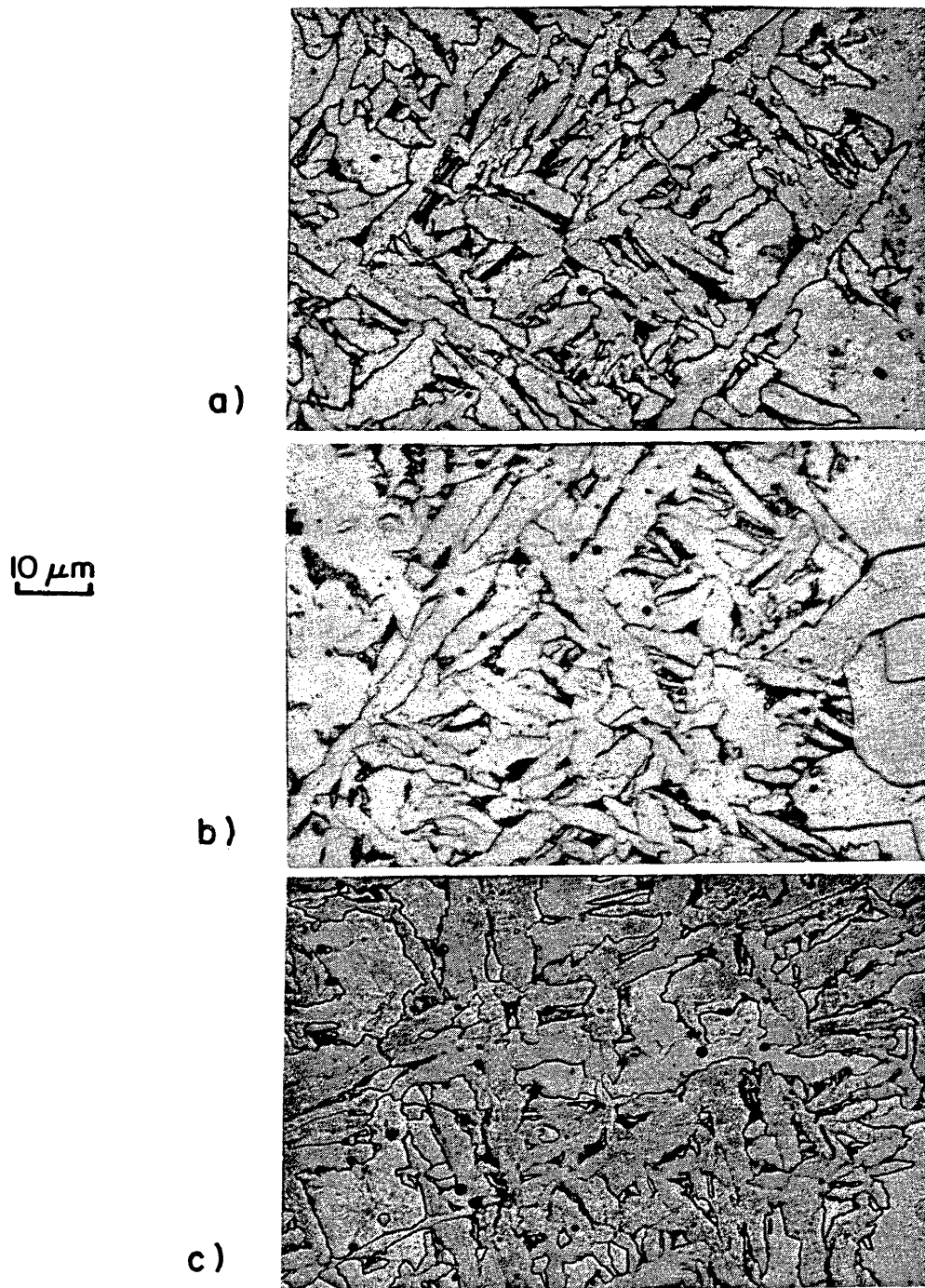


Figure 11. Typical microstructures for regions of acicular ferrite are shown for fine austenite grained samples in the a) -1.0 (compression) normalized loading condition, b) no load condition and +1.0 (tension) loading condition.

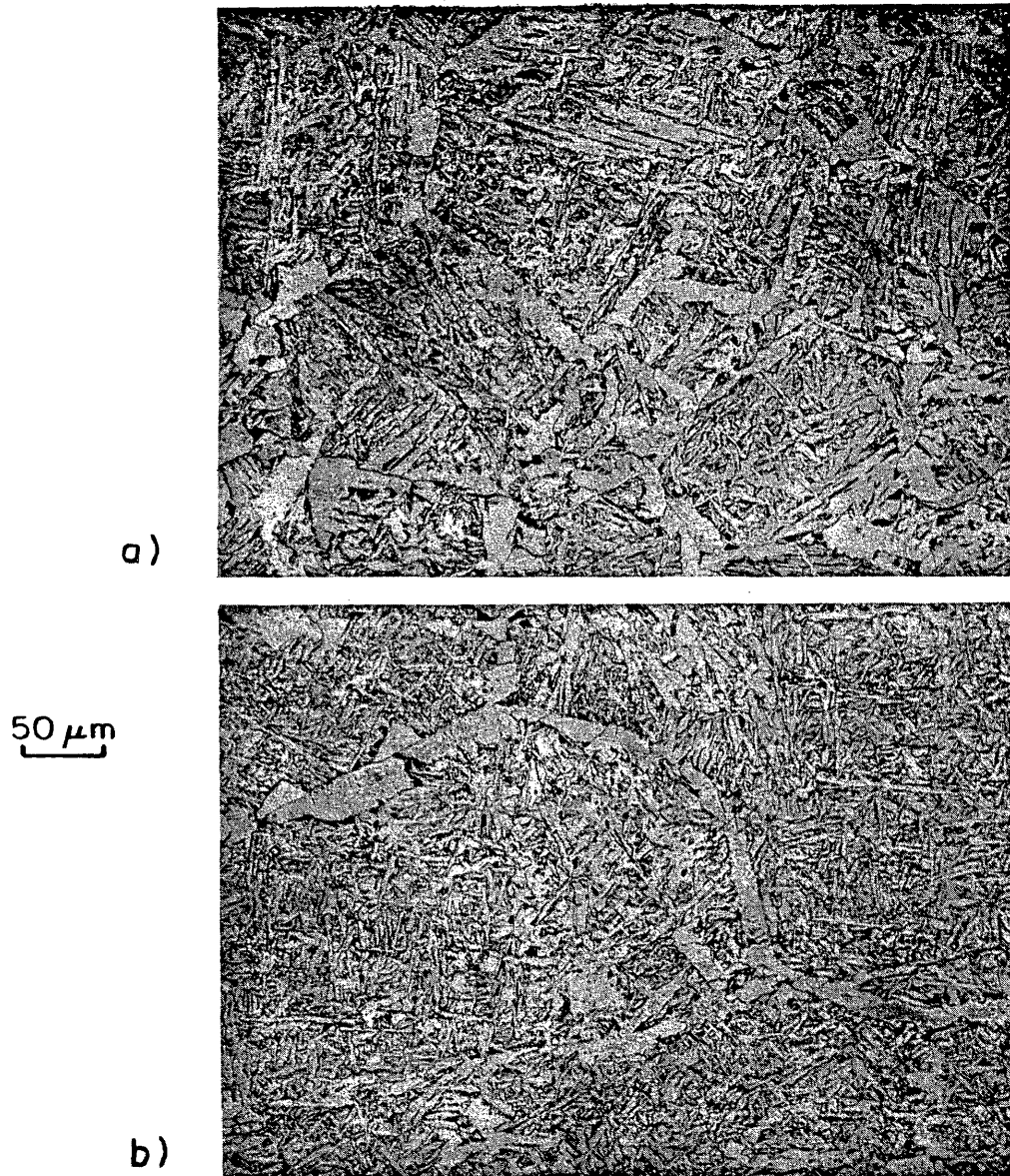


Figure 12. Typical microstructures are shown for a) the fine grained austenite tests and b) the coarse grained austenite tests.

were applied, and an acicular ferrite lath size of 3.27 μm resulted. This sample plastically deformed during the test and produced extremely large austenite grains. The average austenite grain size is over 450 μm although there were a few very large austenite grains and several small ones. The average acicular ferrite lath size was the lowest of any sample seen in this study. The darkened point in the lower right of Figure 10 is for this sample.

Figure 13 shows how the prior austenite grain size varied in the range of loading conditions. As the normalized loading approaches +1.0 the austenite grain size begins increase for the "fine" austenite grains.

For each of the samples, the acicular ferrite transformation temperature were identical, within the resolution of the experimental setup. Acicular ferrite began to form at approximately 620°C in each of the loading conditions.

Results of quantitative metallographic analysis are presented in Figures 14 through 16 for these "fine" grained austenite tests. The microstructure is quantified here into only three categories, allotriomorphic (grain boundary) ferrite, acicular ferrite, and aligned ferrite, which includes both Widmanstatten ferrite and bainitic constituents. As the first approximation, the microstructure was divided as around forty percent of allotriomorphic ferrite and roughly thirty percent each of aligned ferrite and acicular ferrite.

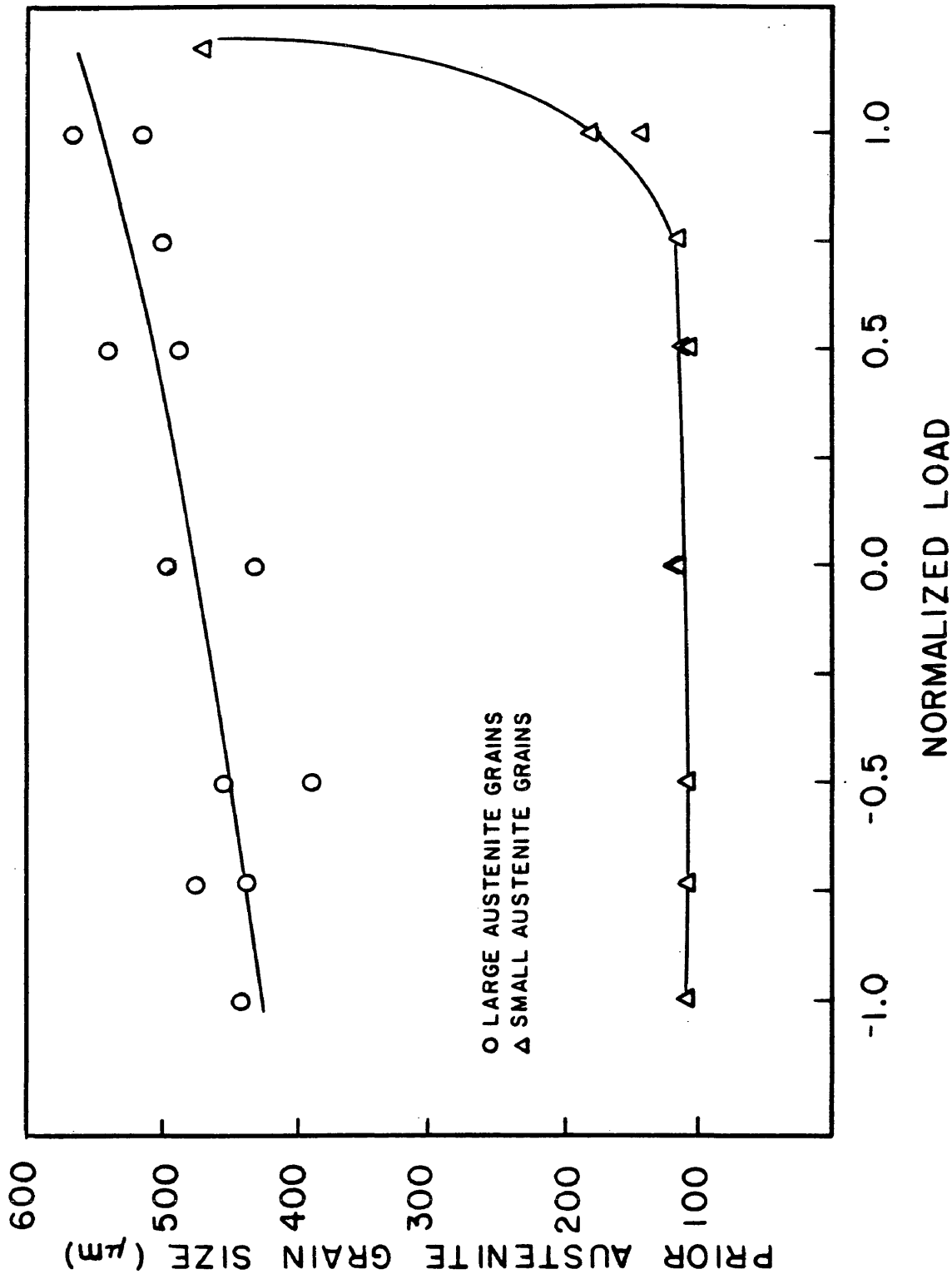


Figure 13. The prior austenite grain sizes are shown for the "fine" and "coarse" grained austenite samples.

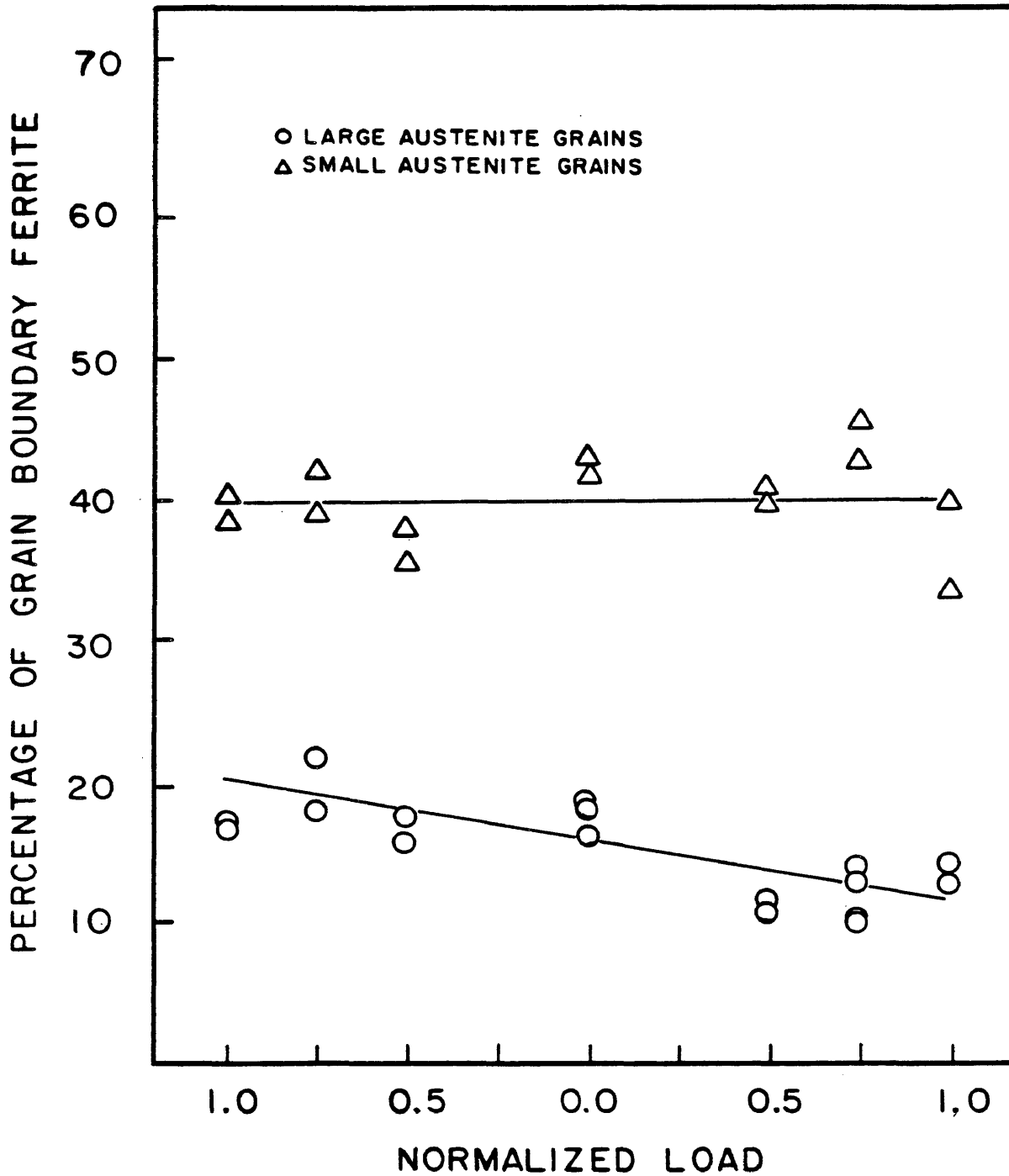


Figure 14. The variation of percentage of the microstructure comprised of grain boundary ferrite is shown for the different loading conditions.

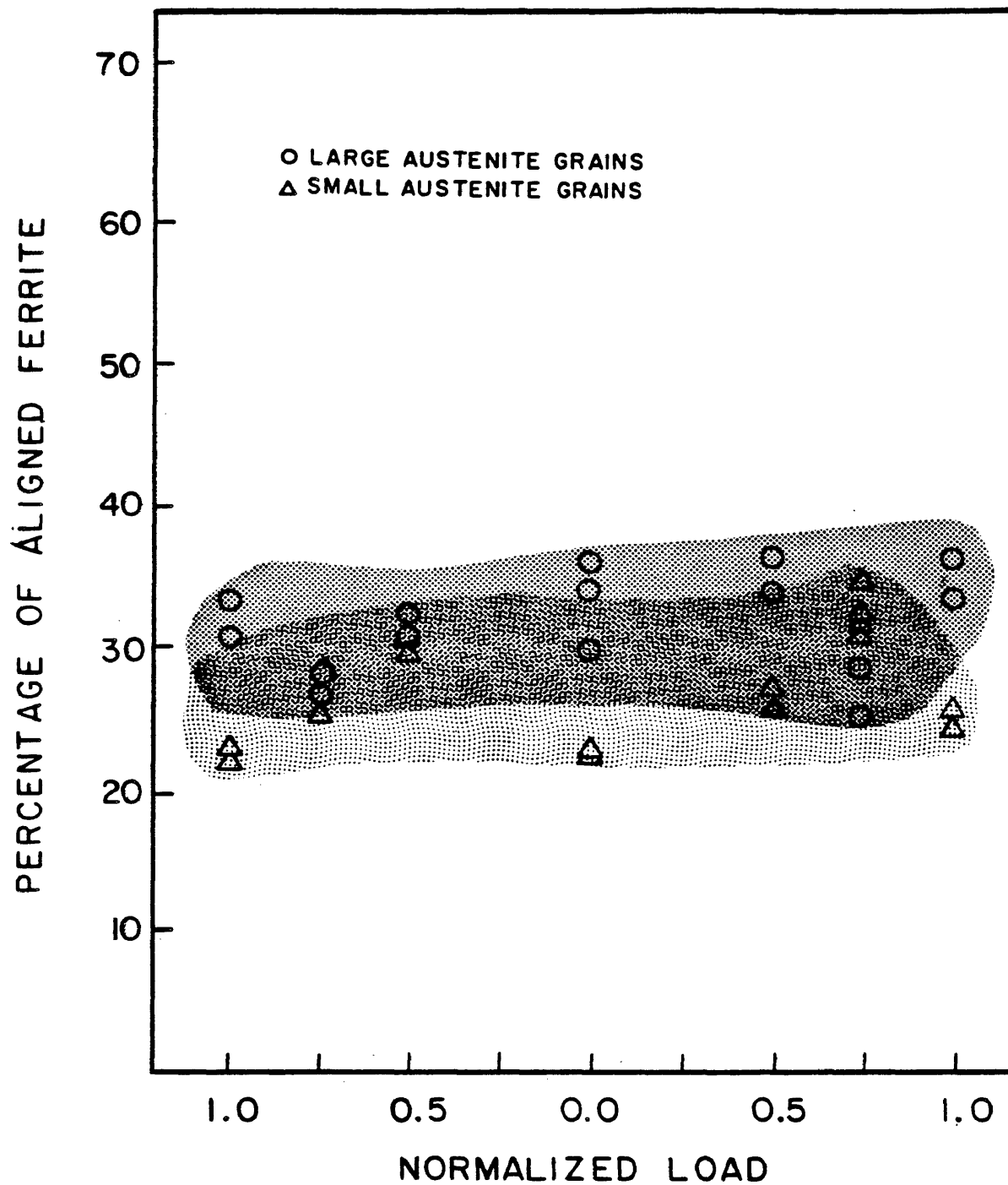


Figure 15. The variation of aligned ferrite is shown for the different loading conditions.

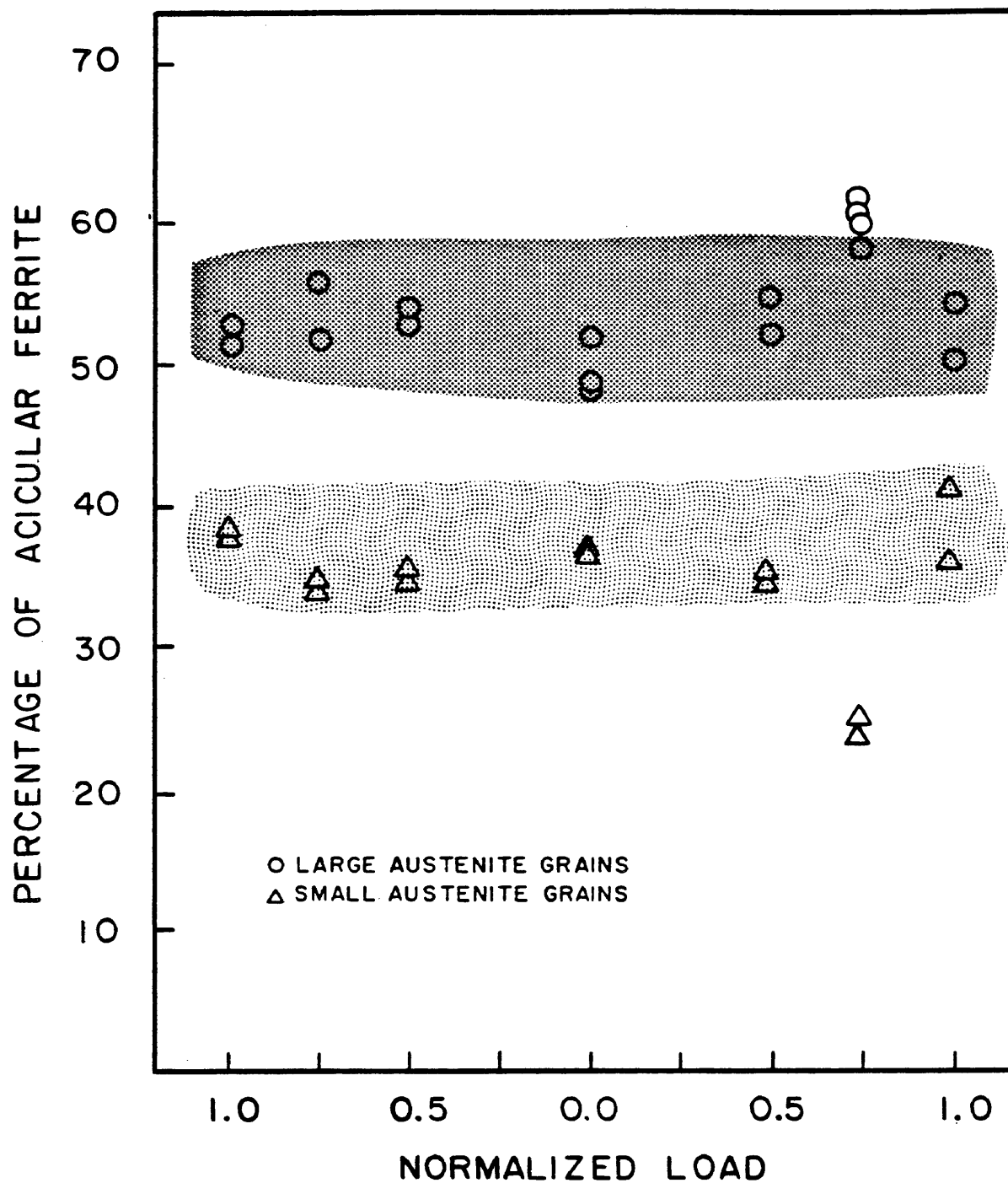


Figure 16. At the various loading conditions, the percentage of acicular ferrite in the microstructure is shown for the two austenite grain size conditions.

B. Coarse Grain Austenite Tests

Referring back to Figure 10, the acicular ferrite lath size is given in the lower curve for the various loading conditions for tests where larger austenite grains were grown. All of the acicular ferrite lath size values are reasonably close, but, as was the case with the fine austenite grain tests, there seems to be a trend of decreasing lath size as the normalized loading condition varies from the no load condition. The average lath size in the -1.0 loading condition was around 3.8 μm , while in the no load condition, the average lath size was about 4.5 μm and it drops to roughly 4.0 μm for the +1.0 loading condition.

Microstructures of the large austenite grain size specimens are shown in Figures 12b and 17. The prior austenite grain sizes are shown in Figure 13 for the "large grain austenite" tests. All were around 500 μm , although the prior austenite grain size increases from slightly above 400 μm the -1.0 loading condition to over 500 μm in the +1.0 loading condition.

Results of quantitative metallographic analysis are presented in Figures 14 through 16. Whereas in the "fine" grain austenite tests, there was approximately one third acicular ferrite, in these "large" grain austenite tests, the proportion of acicular ferrite was uniformly greater than fifty percent. The amount of aligned ferrite was slightly higher in the "coarse" grain austenite than in the "fine" grain austenite tests, and this is independent of loading conditions.

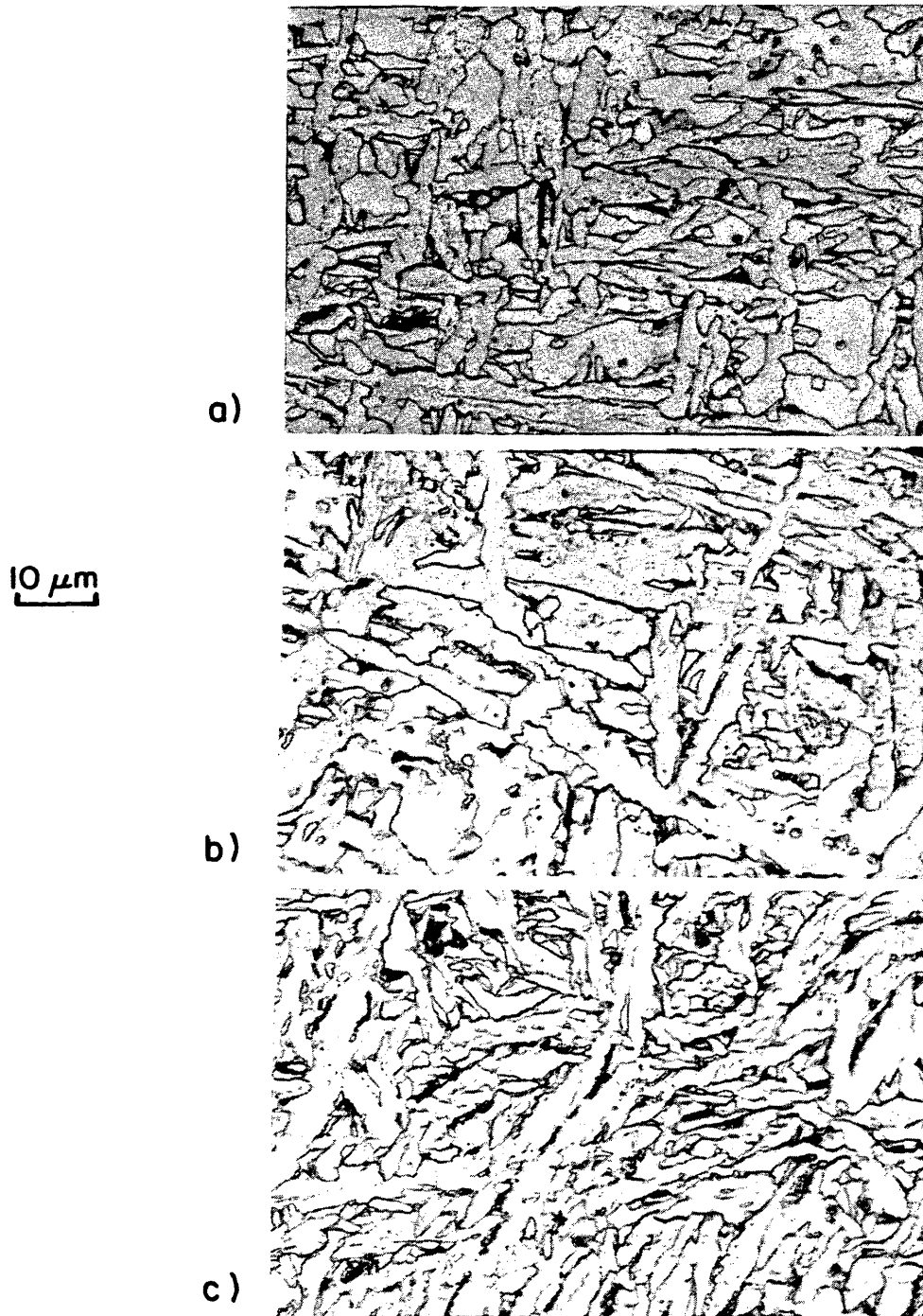


Figure 17. Regions of typical acicular ferrite in the large austenite grain size samples are shown. The compressive loading cycles of -1.0 normalized load is shown in a) in b) the no load condition is shown and in c) is the +1.0 normalized loading condition.

The acicular ferrite transformation temperatures in these tests were once again very nearly indistinguishable. Within the resolution of the dilatometer data, the temperature at which acicular ferrite began to form was approximately, regardless of loading condition 590°C. This is in contrast to approximately 620°C in the earlier tests.

The thickness of grain boundary ferrite film thickness was independent of either the austenite grain size or the loading condition, as shown in Figure 18. This, in conjunction with Figure 13, the austenite grain size is consistent with the quantitative metallography showing the decrease in fraction of grain boundary ferrite as the loading condition tends towards +1.0 in figure 14.

One additional factor which is of interest is related to the microstructure which is not grain boundary ferrite. This is now the "residual" microstructure is divided into acicular ferrite and aligned ferrite. Figure 19 shows the percentage of acicular ferrite inside the grain boundary ferrite "envelopes". While not universally higher, the large grained austenite tends to occupy a higher percentage of the "remaining microstructure" than does the fine austenite. The transformation temperatures for the acicular ferrite and Widmanstätten (aligned) ferrite are very close. The "residual" microstructure should then show similar transformation behavior. One qualification should be placed on this statement. Widmanstätten ferrite requires a substrate existing ferrite, so some austenite grain size should be felt.

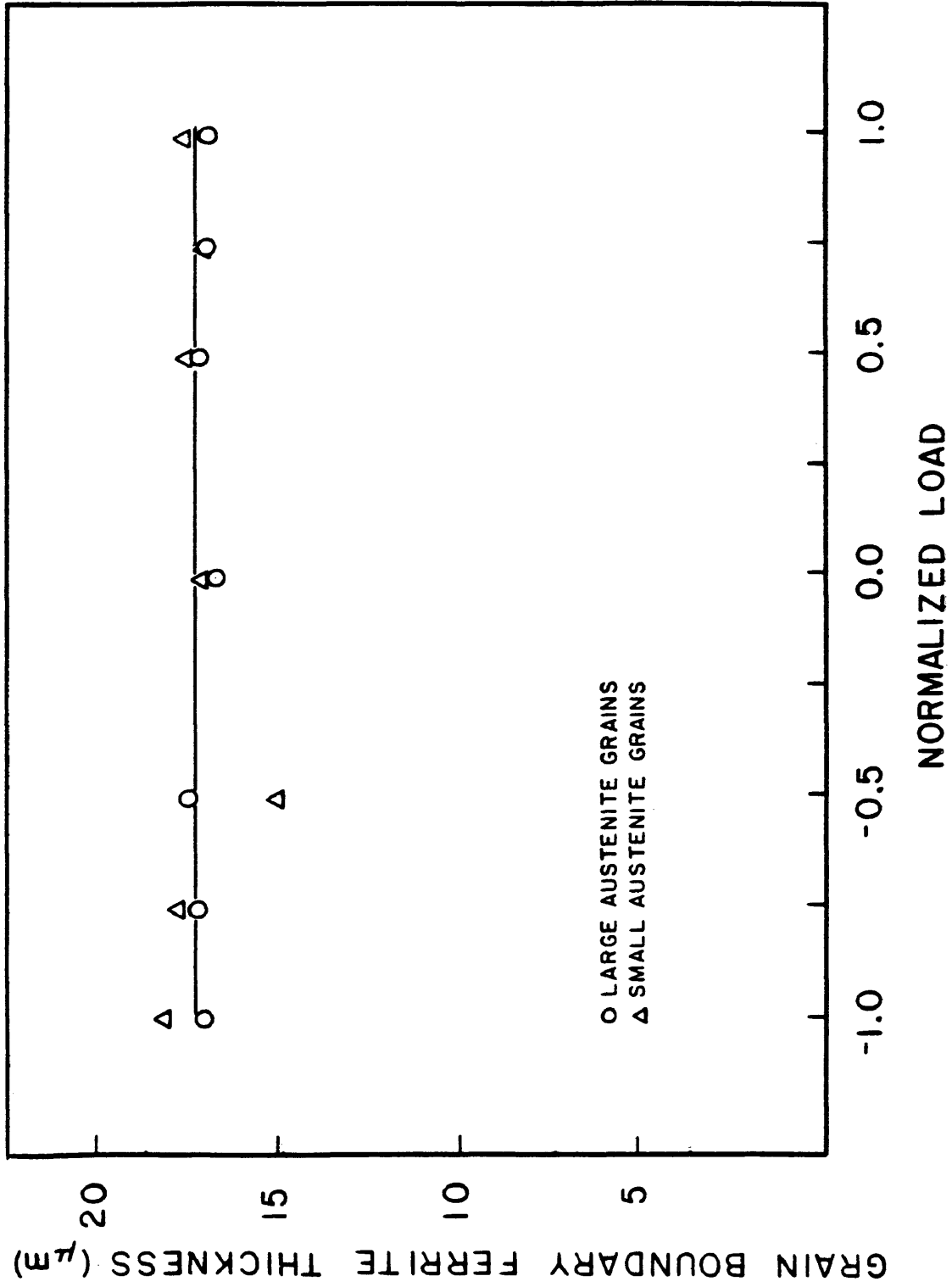


Figure 18. The variation of grain boundary ferrite thickness is presented for the different normalized loading conditions and austenite grain sizes.

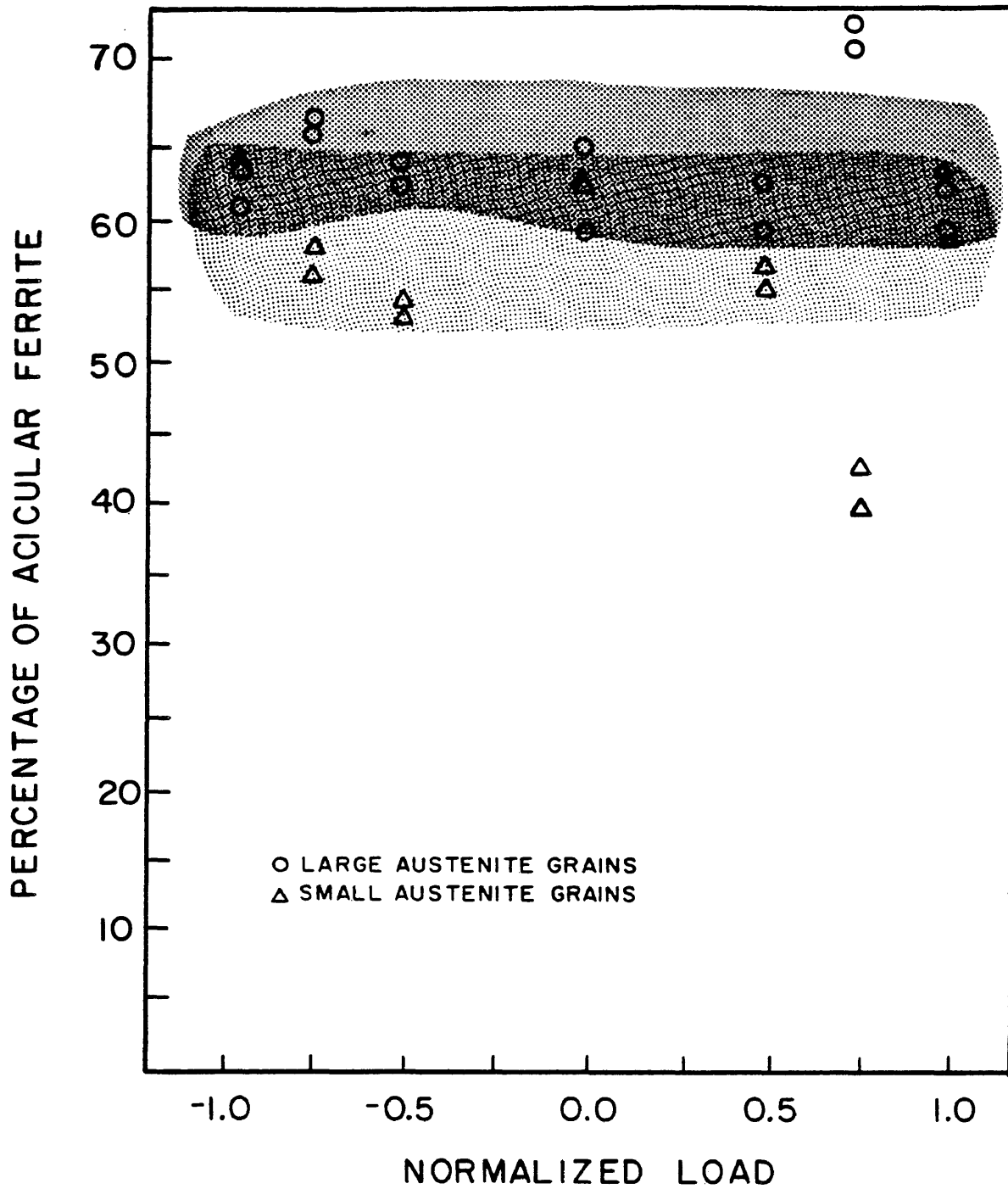


Figure 19. The microstructure of the samples was made up of grain boundary ferrite, acicular ferrite and aligned ferrite. Discounting the grain boundary ferrite, the amount of acicular ferrite is shown.

C. Summary of Results

- Much finer acicular ferrite resulted when the acicular ferrite formed inside large austenite grains than when it formed inside fine austenite grains.
- For acicular ferrite formed in the "fine" grain austenite tests, there is a small trend of decreasing acicular ferrite lath size as the load is increased in either the tensile or compressive direction.
- A similar trend was seen in the "coarse" austenite tests, where loading cycles in either tensile or compressive directions slightly decrease the acicular ferrite lath size.
- Acicular ferrite start temperatures were insensitive to loading condition, but were lower in "coarse" grain austenite than in "fine" grain austenite.
- In "fine" grain austenite tests, the microstructures contained around forty percent grain boundary ferrite, and roughly thirty percent each of the aligned constituent and acicular ferrite. "Coarse" grain austenite transformed to over fifty percent of acicular ferrite. Of the remaining microstructure, there was more aligned ferrite than grain boundary ferrite.
- The "residual" microstructures are nearly identical for "coarse" and "fine" grain austenite.

IV. DISCUSSION

A. Nucleation in an Unstressed System

The idea under examination is whether the acicular ferrite phase transformation or nucleation are altered by applied loads of the magnitude attainable in welding. Devalliers (33) originated this idea, suggesting that thermal contraction differences between an austenite matrix and inclusions set up local high energy regions that may act as preferential sites for ferrite nucleation. By macroscopically loading austenite in this investigation, the effectiveness of these preferential sites for nucleating acicular ferrite is being evaluated.

Modeling of the assumed process begins with classical nucleation theory. A scheme can be derived whereby the acicular ferrite nucleation rate is related to experimental variables. Next, the classical nucleation rate expression is modified to account for the effects of applied loads or imposed strains. The net effect of the strain energy applied can be characterized by the results compared to the modified nucleation theory.

From classical nucleation theory, the nucleation rate, I , is given by the equation:

$$I = \nu \cdot 0_c \exp \frac{-\Delta G^0}{RT} N_0 \frac{-\Delta G^*}{RT} \left(1 - \exp \frac{-(\Delta G^0 + \Delta G_v)}{RT} \right) \quad (35)$$

Where ν is the frequency of atom jumps, O_c is the number of atoms in a position to make a jump into the forming nucleus, N_0 is the total number of possible nucleation sites per unit volume, ΔG^0 is the activation energy barrier facing any atom attempting to jump into the nucleus, and ΔG^* is the activation energy barrier to the formation of a new critically sized nucleus. The volumetric free energy change of the reaction is ΔG_v . The term in parenthesis is to account for back jumps and can be ignored with large ΔG_v . In some cases, to account for an incubation time to nucleate, an addition factor is added to this equation.

$$I_0 = I \exp \frac{-\tau}{t} \quad (36)$$

where τ is the incubation time. I_0 is the corrected nucleation rate. The term τ is used to account for the time required to reach a steady state nucleation rate (66).

Figure 20 is a diagram of what the ΔG barriers represent. By going from state 1 (austenite) to state 2 (ferrite), an atom must overcome the activation energy barrier ΔG^0 . This is a kinetic barrier to nucleation. By going from state 1 to 2, the total free energy of the system is lowered by ΔG_v . However, in the nucleation rate equation, the volumetric free energy change is not used, but instead ΔG^* is used. The term ΔG_v is the thermodynamic drive for a reaction to proceed. Figure 1 shows

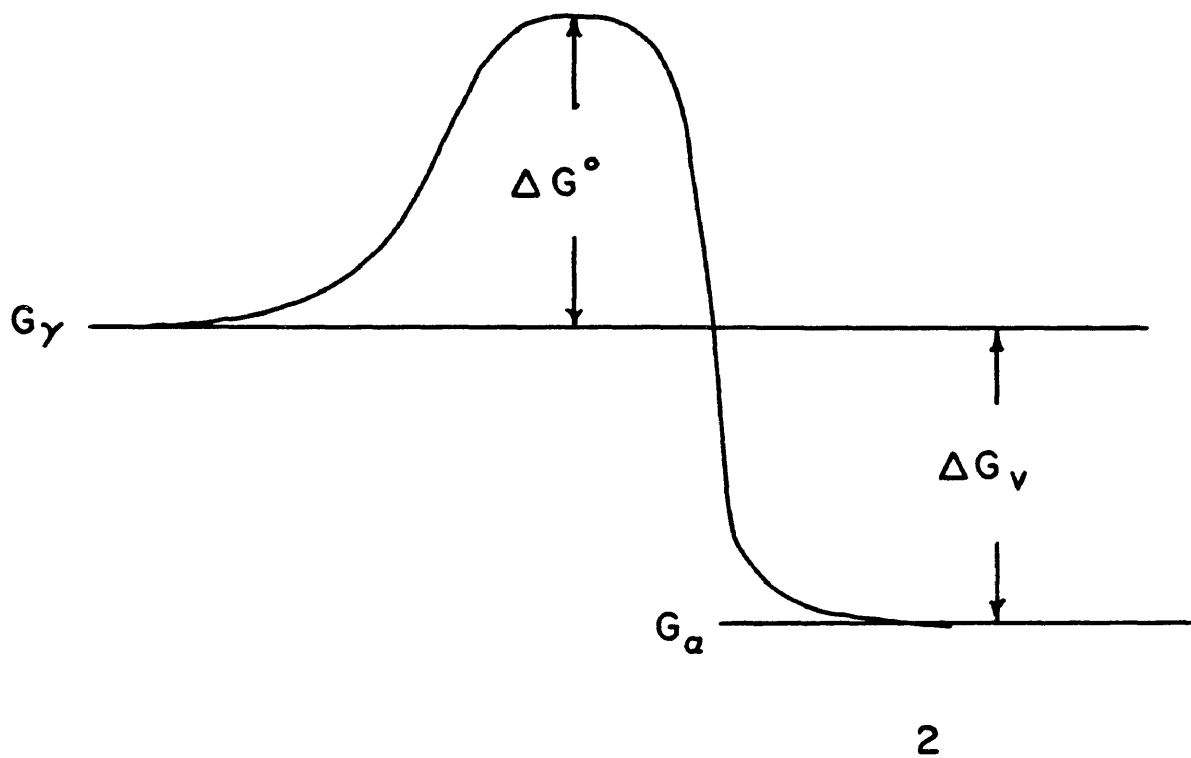


Figure 20. A schematic diagram is presented of free energy versus reaction coordinate. State I is austenite which has G_γ , State II is ferrite with a free energy of G_α . The driving force for reaction is ΔG_v while the atoms passing from austenite to ferrite must overcome the barrier of ΔG° .

ΔG^* , which is related to the driving force for the reaction to proceed and also the energy required to form an interface between the nucleus and the matrix. This term, ΔG^* , is a measure of how difficult it is to form a nucleus. Earlier, ΔG_v the volumetric free energy change, was related to the activation energy barrier to nucleation through the following equation:

$$\Delta G^* = \frac{AY^3}{\Delta G_v^2} \quad (37)$$

With the assumption of no temperature dependence of either the enthalpy or entropy, ΔG_v is equal to the degree of undercooling times the enthalpy change, ΔH , divided by the equilibrium temperature, and the form of the nucleation energy barrier to nucleation becomes:

$$\Delta G^* = A \gamma^3 \left(\frac{T_{eq}}{\Delta H \Delta T} \right)^2 \quad (38)$$

B. Nucleation With Strain Energy

When accounting for the effect of the applied strain energy, the work can be assumed to be additive to the volumetric free energy change, ΔG_v . There is an additional strain energy term which has been ignored to this point, this being the strain energy associated with the phase transformation itself. Now, the total "new" driving force, ΔG_s , is the sum of the volumetric free energy change, ΔG_v the transformation strain energy, ΔG_t ,

and the contribution due to the applied loads, ΔG_a . In equation form, this is:

$$\Delta G_s = \Delta G_v + \Delta G_t + \Delta G_a \quad (39)$$

Each of the strain energy terms will impart their own influence on ΔG_s .

This is the "new" driving force for reaction, and will be related to activation energy that accounts for strain energies, as follows:

$$\Delta G_s^* = \frac{A\gamma^3}{(\Delta G_s)^2} \quad (40)$$

It is presumed that ΔG^* and ΔG_s^* will be different, and ultimately the microstructure will reflect the variations in ΔG^* .

If nucleation is the critical step in the formation of acicular ferrite, and the growth rate is assumed to be constant, the fineness of acicular ferrite microstructure should be a measure of the nucleation rate.

Now nucleation rate expressions will be written for both the stressed and unstressed conditions.

$$I_s = K \exp \frac{\Delta G_s^*}{RT} \left(1 - \exp \frac{-(\Delta G^\circ + \Delta G_s)}{RT} \right) \quad (41)$$

and for the unstressed case:

$$I_o = K \exp \frac{\Delta G^*_o}{RT} \left(1 - \exp \frac{-(\Delta G^\circ + \Delta G_v)}{RT} \right) \quad (42)$$

where the subscript o will now signify a stress free system.

With appropriate assumptions regarding the magnitude of the driving force, this can be reduced to:

$$\frac{I_s}{I_o} = \exp \frac{-\Delta G^*_s - \Delta G^*_o}{RT} \quad (43)$$

If, as was assumed in Equation 37, the thermodynamic driving force for a reaction can be expressed in terms of a required undercooling for nucleation, ΔT , the following expression results.

$$\frac{\Delta G^*_s}{\Delta G^*_o} = \frac{(\Delta T_o)^2}{(\Delta T_s)^2} \quad (44)$$

Equation 43 can now be simplified to:

$$\frac{I_s}{I_o} = \exp \Delta G^* \left(1 - \left(\frac{\Delta T_s}{\Delta T_o} \right)^2 \right) \quad (45)$$

The assumption will now be made that the number of acicular ferrite laths per unit volume, N , is indicative of the nucleation rate. The acicular ferrite size implies that the growth rate is not important in determining the microstructure. Mathematically, this is given as:

$$\frac{I_s}{I_o} = \frac{N_s}{N_o} = \left(\frac{d_o}{d_s}\right)^3 \quad (46)$$

With a high nucleation rate, a fine acicular ferrite lath size would be expected, while a coarse microstructure should result from a low nucleation.

Inserting equation 46 into equation 45, and taking logarithms:

$$\ln \frac{N_s}{N_o} = 3 \ln \frac{d_o}{d_s} = \frac{\Delta G_o^*}{RT} \left(1 - \left(\frac{\Delta T_s}{\Delta T}\right)^2\right) \quad (47)$$

This is a form that consists of quantities which can be experimentally measured.

An interesting use of this equation is to insert in some experimental data. If the largest and smallest values of acicular ferrite lath size are inserted, and an approximation of ΔG_o^* is made the expected undercooling can be estimated. Undercooling differences of greater than 10°C would not be expected. This was seen experimentally. The resolution for determining critical temperature on the Gleeble thermal-mechanical testing machine is probably not better than 10°C under ideal conditions.

C. Expected Results

The most fundamental idea under investigation is how ΔG^* $f(g)$, the activation energy barrier to heterogeneous nucleation, can be altered by applied stresses in welding. This must be measured in terms of experimental variables, and the only ones available are 1) the average acicular ferrite lath size, 2) the volume fractions of the various microstructural constituents, and 3) the temperatures at which the acicular ferrite transformation commences.

The acicular ferrite transformation is assumed to be controlled entirely by nucleation upon inclusions, and that the growth rate is constant. The average size of acicular ferrite laths is used as a measure of nucleation rate. The only means of changing the average lath size is by changing the nucleation rate.

In weld metal, there is a certain distribution of inclusions. Each inclusion has a certain ability to nucleate ferrite which is represented by its particular ΔG^* $f(g)$. When the total thermodynamic driving force dictates that a certain distribution of inclusions have met the heterogeneous nucleation criterion, acicular ferrite begins to form on these locations.

Other nucleation sites exist in the weld metal, perhaps with high ΔG^* values. These may be other inclusions of different sizes or compositions, or different regions on the faces of the initial nucleating inclusions. In the presence of stress or strain energy, any potential nucleation sites might be altered so they might be either more or less effective.

The problem is to determine how $\Delta G^* f(g)$ is affected by strain energy. By examining Equation 8:

$$I = v_0 \exp \frac{-\Delta G^0}{RT} \exp \frac{-\Delta G^* f(g)}{RT} \quad (8)$$

and assuming that the only quantities that can be changed by strain energy are ΔG^* and the geometric factor $f(g)$ and also that the nucleation rate is represented by the lath size, it becomes clear that whether the average acicular ferrite lath size increases or decreases depends on how ΔG^* is changed.

There are two ways of viewing this situation, most easily described with the aid of equation 6:

$$\Delta G_s^* = \frac{A\gamma^3}{(\Delta G_v + \Delta G_T + \Delta G_A)^2} \quad (6)$$

where the terms are as described earlier. The quantity ΔG_v is independent of stress, and is always negative. The transformation strain energy, ΔG_T is constant for an alloy system and is independent of stress. The sign on ΔG_A , the applied strain energy, determines whether ΔG^* increases or decreases.

The first of two possibilities that will be discussed is based on the analysis of Eshelby (52), Lee et al. (56,62) and Morris et al. (65) showed that the strain energy should always be a positive

quantity and consequently lower ΔG_s^* . This is illustrated in the equations 20, 24, 29 and 33.

Operating now under the assumption that strain energy always decreases the total barrier to nucleation $\Delta G^*(f(g))$. The expected results can be stated. Once again, Equation 8, the classical nucleation rate and Equation 48 relating the lath sizes to nucleation rates must be considered.

Loading conditions in either tension or compression will lower the barrier to nucleation, so the nucleation rate will be greater. The consequences of this are: 1) the average acicular ferrite lath size should decrease with increases in loading in either tension or compression, 2) if there is any change in acicular ferrite transformation temperature with loading conditions, it should increase. 3) The volume fraction of acicular ferrite should correspondingly increase at the expense of grain boundary ferrite.

An alternate means of anticipating these same results to examine the effects of uniaxial stresses on a local scale. There is very little difference between tension and compression. The flow of the matrix around austenite inclusions (nucleation sites) is very similar in either case. The direction of flow may be opposite, but the magnitude of strains and the effects of flow should be identical for equivalent magnitudes of stress, regardless of sense.

Another way of anticipating results is by analyzing the two groups of existing literature. They are broken into two classes -

uniaxial stresses effect on the decomposition of austenite, and also the effects of hydrostatic compression on austenite decomposition.

Most of the work done with uniaxial tension has given the result that the time to nucleate decreases, which is essentially the same as a lower nucleation rate, and in continuous cooling the transformation occurs at higher temperatures or shorter times. This is consistent with uniaxial tension lowering the barrier to nucleation.

Hydrostatic compression, as shown in Figure 21 from Nilan, retards the nucleation of ferrite/pearlite. The A1 temperature decreases with pressure, and the transformation curves are pushed to longer times. This is consistent with an increase in the difficulty to nucleate $\Delta G^*(f(g))$. This is in contrast to the other analyses.

Microstructurally, this should give the following results: 1) the average acicular ferrite lath size should become progressively coarser as the stress tends towards large values of compressive stress. 2) If any changes are seen in the acicular ferrite transformation temperature, tensile stresses should increase the transformation temperature and compressive stresses should decrease the transformation temperature, and 3) increasing compressive stresses should correspondingly provide for lower fractions of acicular ferrite.

The magnitude of stresses in welding are much lower than those used in the references cited, particularly the hydrostatic

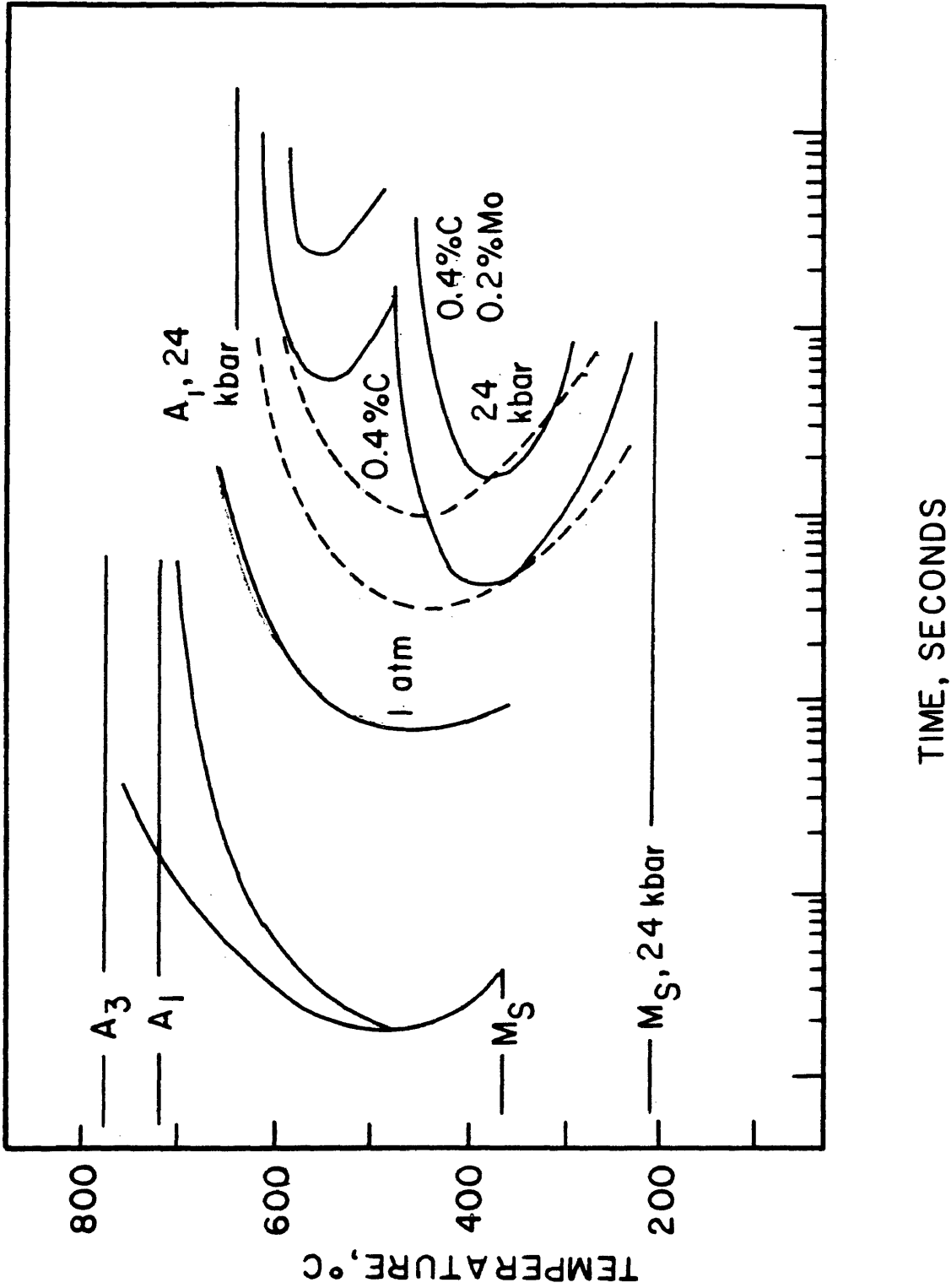


Figure 22. This CCT diagram, after Nilan (49), shows how high compressive stresses push the transformation curves to longer times and lower temperatures.

compression tests. The hydrostatic component of stress in a uniaxial compression test is very low.

It is important to present at least an approximation of the magnitude of the applied strain energy to see if it is sizeable. Using the method of Lee et al. (61) the magnitude of the strain^o energy corresponding to the applied stresses can be estimated. While the plastic work related to the applied stresses could be several percent of the volumetric free energy change, ΔG_v , strain energy which could be attained would be only 2% as large as the volumetric free energy.

The applied strain energy therefore may or may not be significant when viewed in comparison to the volumetric driving force. Since the effect is in an exponential term, it may be significant. In any case, the effect of stresses of the magnitude used would not be expected to have a large effect on the nucleation.

D. Comparison of Predicted to Actual Results

The assumption has been made that nucleation controls the microstructure of acicular ferrite, and the growth rate is nearly constant. The justification for this experiment comes from Figure 18 showing the grain boundary thickness in various loading conditions. This figure shows that the growth rates of allotriomorphic ferrite are independent of loading condition. If acicular ferrite grows by the same mechanism as allotriomorphic

ferrite, this would be good justification of the nucleation assumption.

There were no strong trends in the acicular ferrite lath size at different loading conditions, Figure 11. While it may not be significant, for either tensile or compressive loading cycles it appears that the average acicular ferrite lath size decreases with increased loading, without regard to austenite grain size. This is consistent with the theories of Eshelby, Lee and Morris where the sense of stress is unimportant. Strain energy serves to reduce the heterogeneous barrier to nucleation $\Delta G^*(f(g))$.

Within a grain size, the transformation temperature does not change, and the volume fractions of acicular ferrite remain unchanged.

E. The Influence of Austenite Grain Size

One of the principal results found in this study is that acicular ferrite formed from large austenite grains tends to be fine, while acicular ferrite formed from small austenite grains tends to be relatively coarse. This is evident from Figure 10 and also from the replotted data of Fleck (26) in Figure 22.

From this, it is apparent that the acicular ferrite phase transformation is tied in with the other ferrite transformations with which it competes.

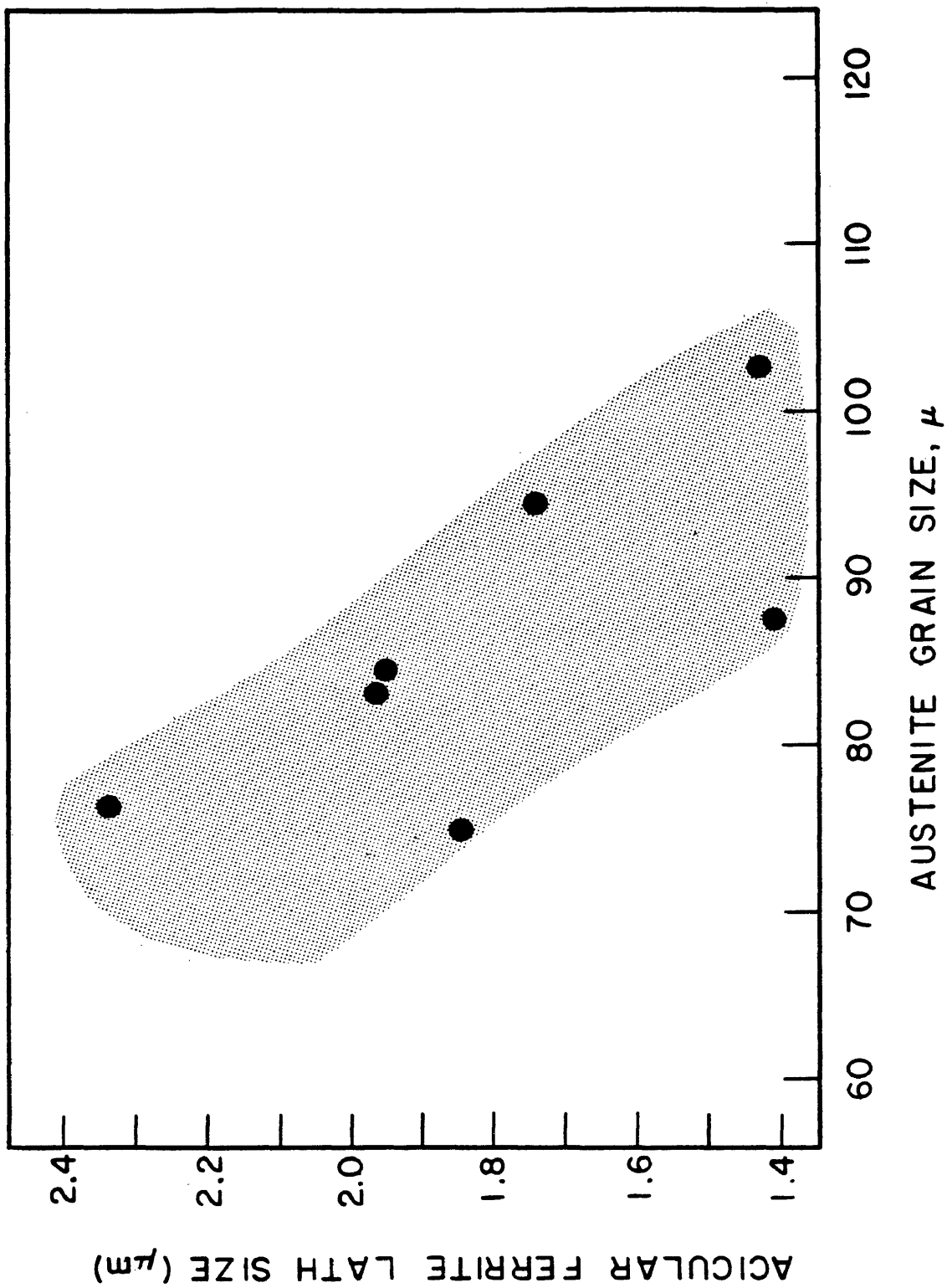


Figure 23 The variation of acicular ferrite lath size with austenite grain size is given for the data of Fleck (26).

In a single weld, there is a certain distribution of nucleation sites (inclusions), and in a macroscopic sampling area there is a uniform composition. Conditions for the acicular ferrite nucleation should be identical for the large and fine austenite grain sizes utilized here.

In low carbon steel weld metal, as the material cools, the allotriomorphic (grain boundary) ferrite formation eventually commences. This ferrite grows to a certain thickness prior to the start of the acicular ferrite transformation. As shown in Figure 20, the grain boundary ferrite film thickness is nearly identical for both large and small austenite grain sizes with a fixed cooling rate and was independent of loading condition. At this point in the cooling cycle, there are volumes of austenite surrounded by grain boundary ferrite. The austenite in either of the grain sizes should be identical, whether it is a large volume of austenite or a small volume. This austenite will transform to either acicular ferrite or an aligned ferrite component. If the acicular ferrite transformation is independent of the competing ferrite transformations, the acicular ferrite forming from either austenite grain size should be identical and should occur at the same temperature.

What actually happens is that when the different volumes of austenite transform to acicular ferrite, it forms acicular ferrite of different lath sizes depending on the prior austenite grain

size. Since the Widmanstätten ferrite forms at temperatures higher than the acicular ferrite, there is a possibility that the acicular ferrite transformation is affected by either the Widmanstätten transformation or the grain boundary ferrite transformation.

In the "fine" grain austenite tests, the acicular ferrite forms at around 620°C and is relatively coarse. Relatively fine acicular ferrite forms between 590°C and 600°C in the "coarse" austenite grains.

Based on the apparent transformation temperatures above, it would be expected that the fine grained austenite would yield coarser acicular ferrite than the coarse grained austenite. For nucleation and growth transformations, finer microstructures are obtained up to a point with decreasing temperatures because of the temperature dependence of the nucleation rate and the growth rate. The ratio of nucleation rate to growth rate increases as the temperature is lowered below the equilibrium temperature.

These transformation temperatures are not necessarily precise because the formation of Widmanstätten ferrite in the "fine" austenite tests may be altering the dilatometer output used to determine the transformation temperatures.

The question naturally arises as to why the transformations are not identical. Some possible explanations exist, and will be discussed. These include "self loading", "hardenability" and a latent heat model.

The first possibility mentioned was "self loading". The essence of this model is that when the ferrite layer forms on the austenite boundaries, the volumetric expansion produces compressive loads in the remaining austenite. The compressive stress state would be much greater when the ratio of grain boundary ferrite thickness to austenite grain size is large. Thick films around small grains would cause higher compressive stresses than thin films of ferrite around large austenite grains.

A point to be made for this model is that with extremely large austenite grain sizes, the effects of the transformation loads would be negligible. Although a wide range of austenite grain sizes was not used, there was some variation in the austenite grain sizes in the "coarse" austenite tests. They ranged from 425 to 550 microns as the load varied from the full compressive loading cycle to the full tensile loading cycle.

One problem with this model is that in the "fine grain" austenite tests, the highest compressive loading cycle produced the finest acicular ferrite lath size. Progressively lower compressive loading cycles caused coarser acicular ferrite laths to form. These results contradict what would be predicted based on the "self loading" model.

The next model will be called a "hardenability" model. When grain boundary ferrite forms, alloying elements are partitioned into the remaining austenite, thereby increasing the hardenability of the austenite.

In fine grain austenite samples, the degree or effect of partitioning should be large when compared to large austenite grains. The fine grain samples would then be expected to transform at temperatures lower than the coarse austenite grain samples, and also have a finer acicular ferrite microstructure. The thickness of the grain boundary ferrite would then be larger also. None of these implications is consistent with the results that were actually seen.

A third potential model would be based on the release of latent heat as the grain boundary ferrite forms. If, for instance, this heat were preferentially rejected into the remaining austenite, it is conceivable that the transformation to acicular ferrite would be different in large austenite grain welds than in fine grained austenite. An interesting calculation can be made to see how much of a temperature increase can be attained with a 10 μm grain boundary ferrite thickness in small (50 μm) and large (250 μm) parallelepiped shaped grains. The latent heat could increase the temperature of the remaining austenite in the fine austenite grains by over 25°C, while the large grains could have the remaining austenite increase in temperature by only 5°C. These are upper limit values, based upon all of the heat going to the austenite. This does not account for the heat transfer characteristics of either phase. In solid state transformations, the rate of growth is not limited by the rate at which heat is removed, but instead by how fast elements can be partitioned.

In a sample which is allowed to free cool, if there are small austenite grains, the latent heat could cause the cooling rate at least on a local level to be lower than if there were large austenite grains. If a certain degree of undercooling and time are required to commence the transformation to acicular ferrite, when longer times are needed to achieve a sufficient undercooling, there is more time for many nuclei to form. This factor would indicate that a fine acicular ferrite microstructure should result with fine austenite grain size when compared with coarse austenite grain size. However, if any nuclei do form at higher temperatures, the opposite would be expected, with fine austenite grain giving rise to a coarse acicular ferrite grain size.

One additional idea which has been examined is the capillarity effect. Many metallurgical phenomena are related to the chemical potential differences arising from curved surfaces as described by the Gibbs-Thompson equation for spheres

$$\Delta\mu = \frac{2\gamma\Omega}{r} \quad (52)$$

where $\Delta\mu$ is the change in chemical potential in crossing the interface, γ is the surface energy, Ω is the atomic volume, and r is the radius of curvature of the sphere.

When appropriate numbers are inserted it becomes clear that the energies associated with either the austenite grain sizes or

allotriomorphs are by orders of magnitude too small to explain the austenite grain size effect.

Each of the models suggested fails to adequately explain fundamentally why the austenite grain size should influence the acicular ferrite lath size. Empirically, the observed transformation temperatures and associated lath sizes are consistent, but the reason the prior austenite grain size causes this change is unclear.

Of the suggested models, the "latent heat" model seems to have the best chance of explaining the results. This would be a difficult model to either prove or disprove because of problems in measuring properties on the 100 micron scale, in particular temperature.

F. Suggested Future Topics

An interesting topic for future study would be the thorough examination of the relationship between austenite grain size and the acicular ferrite transformation.

A test matrix capable of varying the austenite grain size and also the amount of grain boundary ferrite would be required. In this manner the relationship between the various transformations could be studied. In the absence of grain boundary ferrite, the acicular ferrite transformation may not be affected by the prior austenite grain size so changing the amount of grain boundary ferrite (or other constituents) would be desirable.

One factor that has not been mentioned to this point is that nucleus site characteristics may be changing when the austenite grains are grown. In this study austenite grains were coarsened by straining the sample, then holding it at high temperature. The possibility exists that during this processing the inclusions which act as nuclei may be changing. This could bring a change in the nucleation characteristics on the inclusions. This should be considered in any future studies.

G. Summary

A model has been proposed, based upon classical nucleation theory, for the manner in which applied stresses should affect the acicular ferrite phase transformation. This model predicts that tensile stresses should increase the nucleation rate of acicular ferrite, and consequently provide a higher volume fraction of acicular ferrite in the microstructure. Additionally, the tensile stresses should cause the average acicular ferrite lath size to become finer. Compressive stresses, according to the model should have an opposite effects.

Two different austenite grain sizes were utilized - one set at roughly 100 μm and the other with roughly 500 μm austenite grain size. The same trends were found for acicular ferrite lath size in the various loading conditions for acicular ferrite lath size.

The major result is related not to the stress effect, but instead to the effect of austenite grain size. The large austenite grains transformed to relatively fine acicular ferrite lath sizes, while fine austenite grains transformed to relatively coarse acicular ferrite.

No trends were found in the microstructures other than a decrease in the amount of grain boundary ferrite with increasing austenite grain sizes.

V. CONCLUSIONS

1. Applied stresses of the magnitude attainable in welding have very little influence upon the acicular ferrite phase transformation.
2. There seems to be a relationship between the acicular ferrite transformation and competing transformations, most likely the grain boundary allotriomorphic ferrite transformation.

VI. REFERENCES CITED

1. Ahlblom, B., "Oxygen and its Role in Determining Weld Metal Microstructure and Toughness, A State-of-the-Art Review", IIW Report IX-1322-84, 1984.
2. Graville, B.A., "Factors Affecting the Toughness of Submerged Arc Weld Metal Part II", Technology Focus (Welding Institute of Canada), v. 2, London, p. 1 (1980).
3. Abson, D.J., Dolby, R.E., and Hart, P.H.M., "The Role of Nonmetallic Inclusion in Ferrite Nucleation of Carbon Steel Weld Metals", Proc. of an International Conference on "Trends in Steels and Consumables for Welding", The Welding Institute, p. 75 (1978).
4. Cochrane, R.C. and Kirkwood, P.R., "The Effect of Oxygen on Weld Metal Microstructure", Proc. of an International Conference on "Trends in Steels and Consumables for Welding", London, The Welding Institute, p. 103 (1978).
5. Choi, C.L. and Hill, D.C., "A Study of Microstructural Progression in As-Deposited Metal", Welding Research Supplement to the Welding Journal, 57 (8), p. 232s-236s (1978).
6. Ricks, R.A., Howell, P.R., and Barritte, G.S., "The Nature of Acicular Ferrite in HSLA Steel Weld Metals", Journal of Materials Science, v. 17, pp. 732-740 (1982).
7. Keville, B.R. and Cochrane, R.C., "Factors Controlling the Microstructure and Toughness of Submerged Arc Weldments", Hobart, The Australian Welding Institute, Proc. 30th Annual Convention on "Welding Technology 82", (1982).
8. Barritte, G.S. and Edmonds, D.V., "Microstructure and Toughness of HSLA Steel Weld Metals", Proc. of an International Conf., on "Advances in the Physical Metallurgy and Applications of Steels", London, Metal Society, pp. 126-135 (1982).
9. Harrison, P.L., and Farrar, R.A., "Influence of Oxygen Rich Inclusions on the Austenite to Ferrite Phase Transformation in High Strength-Low Alloy (HSLA) Steel Weld Metals", Journal of Materials Science, v. 16, p. 2218 (1981).
10. Ferrante, M., and Farrar, R.A., "The Role of Oxygen Rich Inclusions in Determining the Microstructure of Weld Metal Deposits", Journal of Materials Science, V. 17, p. 3293-3298 (1982).

11. Christian, J.W., "The Theory of Transformations in Metals and Alloys", New York, Pergamon Press 1st Edition, pp. 188-199 414-432 (1965).
12. Evancho, J.W., Staley, J.T., "Kinetics of Precipitation in Aluminum Alloys During Continuous Cooling", Metallurgical Transactions A, Vol. 5 (1), Jan. 1974, pp. 43-47.
13. Grong, O., and Matlock, D.K., "Microstructural Development in Mild and Low Alloy Steel Weld Metals", International Metals Reviews 1986, v. 31 (1), p. 27-48.
14. Garland, J.G., and Kirkwood, P.R., "Towards Improved Submerged Arc Weld Metal", Metal Construction, Vol. 7 (5), pp. 275-283 (1975).
15. Tulliani, S.S., Boniszewski, T., and Eaton, N.F., "Notch Toughness of Commercial Submerged-Arc Weld Metal", Welding and Metal Fabrication, August, 48 (8), pp. 327-339 (1969).
16. Garland, J.G. and Kirkwood, P.R., "A Reappraisal of the Relationship Between Flux Basicity and Mechanical Properties in Submerged Arc Welding", Welding and Metal Fabrication, Vol. 43 (4), pp. 217-224 (1975).
17. Taylor, L.G. and Farrar, R.A., "Metallurgical Aspects of the Mechanical Properties of Submerged Arc Weld Metal", Welding and Metal Fabrication, Weld. Met. Fabr., 1975, 43 (4), 305-10.
18. Thomas, R.D., "Submerged-Arc Welding of HSLA Steels", Metal Progress, Vol. 111 (4), pp. 30-36 (1977).
19. Evans, G.M., "Effect of Manganese on the Microstructure and Properties of All-Weld-Metal Deposits", Welding Research Supplement to the Welding Journal, Vol. 59 (3), pp. 67s-75s (1980).
20. Glover, A.G., McGrath, J.T., Tinkler, M.J., and Weatherly, G.C., "The Influence of Cooling Rate and Composition on Weld Metal Microstructures in a C/Mn and a HSLA Steel", Welding Research Supplement to the Welding Journal, Vol. 56 (9), pp. 267s-273s (1977).
21. Levine, E., and Hill, D.C., "Welding of HSLA (Microalloyed) Structural Steels", ASM, Metals Park, Ohio, p. 402 (1978).
22. Dallam, C.B., Liu, S., Olson, D.L., "Flux Composition Dependence of Microstructure and Toughness of Submerged Arc HSLA Weldments, Welding Journal, v. 64 (5), p. 140s-151s (1985).

23. Koukabi, A.H., North, T.H., and Bell, H.B., "Properties of Submerged Arc Deposits - Effects of Zirconium, Vanadium, and Titanium/Boron", Metal Construction, Vol. 11 (12), pp. 639-642 (1979).
24. Bhadeshia, H.K.D.H., Svenson, L.E., Grefott, B., "A Model for the Development of Microstructure in Low Alloy Steel (Fe-Mn-Si-C) Weld Deposits", Acta. Met., vol. 33, (7), pp. 1271-1283 (1985).
25. Liu, S., "The Role of Non-Metallic Inclusions in Controlling Weld Metal Microstructures in Niobium Microalloyed Steels", Colorado School of Mines Ph.D. Thesis #2923 (1984).
26. Fleck, N.A., Grong, O., Edwards, G.R., and Matlock, D.K., "The Role of Filler Metal Wire and Flux Composition in Submerged Arc Weld Metal Transformation Kinetics", Welding Journal 65 (5), 113-127s, (1985).
27. Ito, Y., Bessyo, K., "Weldability Formula of High Strength Steels Related to Heat Affected Zone Cracking", IIW Doc. IX-631-69, (1969).
28. Liu, S., and Olson, D.L., "The Role of Inclusions in Controlling HSLA Weld Microstructure", Welding Research Supplement to the Welding Journal, Vol. 65 (6), pp. 134s-149s, (1986).
29. Smith, C.S., "Grain Phases and Interfaces: An Interpretation of Microstructure", Trans. AIME, v. 175, p. 15 (1948).
30. Gladman, T., "On the Theory of the Effect of Precipitate Particles on Grain Growth in Metals", Proc. of Royal Society A, v. 294, p. 298 (1966).
31. Ito, Y., and Nakanishi, M., "Study on Charpy Impact Properties of Weld Metals with Submerged Arc Welding", The Sumitomo Search, v. 15, p. 42 (1976).
32. Mori, Homma, Wakabayashi, and Okita, "Characteristics of Mechanical Properties of Ti-B Bearing Weld Metals", Japan, Nippon Steel Corporation, IIW Doc. II, 980, May (1982).

33. Devillers, L., Kaplan, D., et al., "The Effect of Low Level Concentrations of Some Elements on the Toughness of Submerged-Arc Welded CMn Steel Welds", Proc. of an International Conf. on "The Effects of Residual, Impurity, and Microalloying Elements on Weldability and Weld Properties", Abington Hall, Abington, Cambridge, The Welding Institute, pp. P1-1-P1-11 (1983).
34. Brooksbank, D., and Andrews, K.W., "Stress Fields Around Inclusions and Their Relation to Mechanical Properties", Journal of the Iron and Steel Institute, v. 186, pp. 246-255 (1972).
35. Hirth, J.P. and Lothe J., "Theory of Dislocations", McGraw Hill, New York, (1968).
36. Fiore N. and Bauer, C., "Binding of Solute Atoms to Dislocations", Pergamon Press, London, 1st Edition, (1968).
37. Nocke, Jansen and Lenk, "Studies of the Effect of Stress on the Isothermal Transition Behavior of the Hypereutectoid Steel UR38Cr-Mo", Neue Hutte, 21 (8), 468-73 (1976).
38. Walker, D.J. and Honeycombe, R.W.K., "Effects of Deformation on the Decomposition of Austenite: Part I-The Ferrite Reaction", Metal Science, Vol. 12 (10), pp. 445-452 (1978).
39. Smith, Y.E. and Seibert, C.A., "Continuous Cooling Transformation Kinetics of Thermomechanically Worked Low-Carbon Austenite", Metallurgical Transactions, v. 2, pp. 1711-1725 (1971).
40. Priestner, R. and Biring, M.S., "Transformation of Low-Carbon Austenite after Small Plastic Strains", Metal Science Journal, v. 7, pp. 60-74 (1973).
41. Ducoin, A., Klein, G., Marya, S.K., and Le Maitre, F., "Thermal Analysis of the Stress and Temperature Induced Phase Transformations in Steels", Proc. of the 6th International Conf. on "Thermal Analysis", Bayreuth, Federal Republic of Germany, pp. 43-48 (1980).
42. Mutiu, T.A., Kinderman, A.J., and Bernstein, I.M., "The Effects of Concurrent Deformation on the Transformation Kinetics of Austenite to Bainite and on the Subsequent Mechanical Properties of Bainitic and Bainitic-Martensitic Structures", from J.B. Ballance's "The Hot Deformation of Austenite", N.Y., AIME, pp. 410-427 (1977).

43. Bhattacharyya, S., and Kehl, G.L., "Isothermal Transformation of Austenite Under Externally Applied Tensile Stress", Transactions of the ASM, v. 47, pp. 351-377 (1955).
44. Kehl, G.L. and Bhattacharyya, S., "the Influence of Tensile Stress on the Isothermal Decomposition of Austenite to Ferrite and Pearlite", Transactions of the ASM, v. 48, pp. 234-248 (1956).
45. Porter, L.F. and Rosenthal, P.C., "Effect of Applied Tensile Stress on Phase Transformations", Acta Metallurgica, v. 7, pp. 504-514 (1959).
46. Priestner, R., "Strain-Induced γ to α Transformation in the Roll Gap in Carbon and Microalloyed Steel", Thermomechanical Processing of Microalloyed Austenite, Pittsburgh, PA, August 17-19, 1981, The Metallurgical Society/AIME, Warrendale, PA, pp. 455-467 (1981).
47. Umemoto, M., Ohtsuka, H., and Tamura, I., "Transformation to Pearlite from Work-Hardened Austenite", Transactions ISIJ, v. 23, pp. 775-784 (1983).
48. Denis, S., Gautier, E., Simon, A., and Beck, G., "Stress Phase Transformation Interactions: Basic Principles, Modelization and their Role in the Calculation of Internal Stresses", Proc. of an International Conf. on "Calculation of Internal Stresses in Heat Treatment of Metallic Materials", Sweden, Linkoping University, pp. 157-190 (1984).
49. Nilan, T.G., "Austenite Decomposition at High Pressure", "Transformation and Hardenability in Steels", Symposium, Climax Molybdenum Company of Michigan and the University of Michigan, pp. 57-68 (1967).
50. Fujita, M. and Suzuki, M., "The Effect of High Pressure on the Isothermal Transformation in High Purity Fe-C Alloys and Commercial Steels", Transactions ISIJ, v. 14, pp. 44-53 (1974).
51. Radcliffe, S.V., Schatz, M., and Kulin, S.A., "The Effects of High Pressure on the Isothermal Transformation of Austenite in Iron-Carbon Alloys", J. Iron and Steel Inst., London, 201, 143 (1963).
52. Eshelby, J.D., "The Determination of the Elastic Field on an Ellipsoidal Inclusion and Related Problems", Proc. Roy. Soc., v. A241, pp. 376-396 (1957).

53. Eshelby, J.D., "The Elastic Field Outside an Ellipsoidal Inclusions", Proc. Roy. Soc., v. A252, pp. 963-970 (1977).
54. Shelley, J.F., and Yu, Y.Y., "The Effect of Two Rigid Spherical Inclusions on the Stresses in an Infinite Elastic Solid", Transactions of the ASME, Journal of Applied Mechanics, v. 33, pp. 68-74 (1966).
55. Chen, F.C. and Young, K., "Inclusions of Arbitrary Shape in an Elastic Medium", Journal of Mathematical Physics, v. 8, pp. 1412-1416 (1977).
56. Lee, J.K., Barnett, D.M., and Aaronson, H.I., "The Elastic Strain Energy of Coherent Ellipsoidal Precipitates in Anisotropic Crystalline Solids", Met. Trans., v. 8A, pp. 963-970 (1977).
57. Johnson, W.C., Earmme, Y.Y., and Lee, J.K., "Approximation of the Strain Field Associated with an Inhomogeneous Precipitate", Journal of Applied Mechanics, v. 47, pp. 775-780 (1980).
58. Robinson, K., "Elastic Energy of an Ellipsoidal Inclusion in an Infinite Solid", Journal of Applied Physics, v. 22, no. 8, pp. 1045-1054 (1951).
59. Barnett, D.M., Lee, J.K., Aaronson, H.I., and Russell, K.C., "The Strain Energy of a Coherent Ellipsoidal Precipitate", Scripta Met., v. 8, p. 1447 (1974).
60. Shibata, M. and Ono, K., "The Strain Energy of a Spheroidal Inclusion and its Application to bcc-hcp Martensitic Transformation", Acta Metallurgica, v. 23, pp. 587-597 (1975).
61. Lee, J.K., Earmme, Y.Y., Aaronson, H.I., and Russell, K.C., "Plastic Relaxation of the Transformation Strain Energy of a Misfitting Spherical Precipitate: Ideal Plastic Behavior", Metallurgical Transactions, v. II, pp. 1837-1847 (1980).
62. Lee, J.K., Johnson, W., "Influence of Transformation Strain Energy Upon Diffusional Nucleation and Growth", Proceedings of an International Conference on Solid/Solid Phase Transformations, Warrendale, PA, TMS of AIME, 1981.
63. Louthan, M.R., "Stress Orientation of Titanium Hydride in Titanium", Trans. TMS-AIME, 227, 1166, 1963.

64. Hosford, W., and Agrawal, "Effect of Stress During Aging on the Precipitation of θ' in Al-4 Wt. Pct. Cu", Metallurgical Transactions A, vol. 6A (3), pp. 487-499, 1975.
65. Morris, J.W., Khachaturyan, A.G., Wen. S., "The Elastic Contribution to the Thermodynamics of Phase Transformations in Solids", Proceedings of an International Conference on Solid/Solid Phase Transformations, Warrendale, PA, TMS of AIME, 1981.
66. Phase Transformations - Papers presented at a seminar of the American Society for Metals, American Society for Metals, Metals Park, Ohio.

VII. APPENDIX A

The thermal program utilized in the Gleeble tests is presented here. The initial temperature is 1370°C and the time from 500°C to 500°C is 150 seconds.

<u>TIME (secs)</u>	<u>TIME CHANGE (secs)</u>	<u>ACTUAL TEMP. (°C)</u>
5.878	5.878	1345.000
11.866	5.988	1320.000
17.968	6.102	1295.000
24.189	6.221	1270.000
30.534	6.345	1245.000
37.008	6.474	1220.000
43.616	6.608	1195.000
50.364	6.748	1170.000
57.257	6.893	1145.000
64.302	7.045	1120.000
71.507	7.205	1095.000
78.878	7.371	1070.000
86.423	7.545	1045.000
94.151	7.728	1020.000
102.070	7.920	995.000
110.192	8.121	970.000
118.525	8.333	945.000
127.082	8.557	920.000
135.874	8.793	895.000
144.916	9.042	870.000
154.221	9.305	845.000
163.806	9.585	820.000
173.687	9.882	795.000
183.884	10.197	770.000
194.418	10.534	745.000
205.312	10.893	720.000
216.590	11.278	695.000
228.282	11.692	670.000
240.418	12.136	645.000
253.034	12.616	620.000

<u>TIME (secs)</u>	<u>TIME CHANGE (secs)</u>	<u>ACTUAL TEMP. (°C)</u>
266.170	13.135	595.000
279.869	13.699	570.000
294.183	14.314	545.000
309.169	14,986	520.000
324.894	15.725	495.000
341.434	16.540	470.000
358.878	17.444	445.000
377.331	18.453	420.000
396.916	19,586	395.000
417.783	20.867	370.000
440.110	22.327	345.000
464.117	24.007	320.000
490.078	25.961	295.000
518.340	28,262	270.000
549.349	31.010	245.000
583.699	34.350	220.000
622.197	38.498	195.000
665.985	43.787	170.000
716.750	50.765	145.000
777.145	60.396	120.000
851.703	74.557	95.000
949.164	97.461	70.000
1090.174	141.009	45.000
1348.979	258.806	20.000